

# **DESIGN OF A MEASUREMENT SLEEPER**

FOR THE PURPOSE OF VALIDATING MODELS OF BALLASTED  
RAILWAY TRACKS



# **DESIGN OF A MEASUREMENT SLEEPER**

FOR THE PURPOSE OF VALIDATING MODELS OF BALLASTED  
RAILWAY TRACKS

## **Master Thesis**

for the purpose of obtaining the degree of Master of Science  
at the Delft University of Technology,  
to be defended on Monday, 26 July 2021 at 14:30

by

**Remco BOLHUIS**

MSc student Civil Engineering,  
Track Structural Engineering,  
Specialization Structural Mechanics

Delft University of Technology,  
Faculty of Civil Engineering and Geosciences,  
Department of Engineering Structures,  
Section Dynamics of Structures

Composition graduation committee:

Dr. ir. K. N. (Karel) van Dalen,	Delft University of Technology, chairman
A. (Avni) Jain, PhD,	Delft University of Technology, daily supervisor
Prof. dr. ir. A. V. (Andrei) Metrikine,	Delft University of Technology
Dr. ir. P. (Paul) Hölscher,	Deltares, company supervisor

This research is conducted in direct collaboration with Deltares as part of the NWO project *Rapid degradation of railway tracks on soft soils explained and mitigated: multi-scale dynamics modelling, a novel approach* from the TU Delft.



*Keywords:* Instrumented sleeper, Field measurements, Railway tracks, Train-track interaction, Transition zone, Railway track modelling, Dynamic monitoring

An electronic version of this dissertation is available at  
<http://repository.tudelft.nl/>.

# CONTENTS

<b>Summary</b>	<b>vii</b>
<b>Preface</b>	<b>ix</b>
<b>1 Introduction</b>	<b>1</b>
<b>2 Relevant Railway Features</b>	<b>5</b>
2.1 Railway Elements . . . . .	5
2.2 Train Load . . . . .	8
2.3 Behaviour Sleeper. . . . .	9
2.4 Behaviour Ballast . . . . .	12
2.5 Other Mechanisms . . . . .	13
2.6 Conclusion . . . . .	14
<b>3 Product Requirements</b>	<b>17</b>
3.1 Measurements . . . . .	17
3.2 Demands Sleeper . . . . .	18
3.3 Risks . . . . .	19
<b>4 Computational Model</b>	<b>21</b>
4.1 Model Features . . . . .	21
4.2 Results Calculation . . . . .	32
4.3 Conclusion . . . . .	40
<b>5 Measuring Instruments</b>	<b>43</b>
5.1 Matrix Based Tactile Surface Sensors . . . . .	43
5.2 Pressure cells . . . . .	47
5.3 Acceleration Measurements. . . . .	48
5.4 Strain Measurements . . . . .	49
5.5 Conclusion . . . . .	51
<b>6 Design Sleeper</b>	<b>53</b>
6.1 Basic Design Idea . . . . .	53
6.2 Analytical Calculation. . . . .	54
6.3 Ballast-Sleeper Interface . . . . .	57
6.4 Rail-Sleeper interface . . . . .	58
6.5 Acceleration. . . . .	59
6.6 Strain . . . . .	59
6.7 Electrical Resistance . . . . .	60
6.8 Conclusion . . . . .	60

---

<b>7</b>	<b>Implementing Calculations</b>	<b>61</b>
7.1	Ballast-Sleeper Interface . . . . .	61
7.2	Rail-Sleeper Interface . . . . .	63
7.3	Acceleration Measurement . . . . .	65
7.4	Strain Measurement . . . . .	67
7.5	Conclusion . . . . .	68
<b>8</b>	<b>Conclusion</b>	<b>71</b>
	<b>References</b>	<b>73</b>
<b>A</b>	<b>Analytic Calculation</b>	<b>77</b>

# SUMMARY

An important subject in the research on the behaviour of railway structures is the validation of numerical models by means of in-track measurements. Many forms of track measurements have taken place all over the world, mainly in the sense of strain and acceleration measurements, but a more unexplored area is that of the direct measurement of stresses in the ballast.

The aim of this research is to find the best way to equip a railway sleeper with measuring instruments in order to use it for validation of computational models. The sleeper must be able to measure the the vertical velocity of the sleeper as well as the normal stresses on the ballast-sleeper interface over time.

In order to predict the quantities to be measured, a finite element model was build for this research with the Kratos open source software package. The model comprises one single sleeper on top of a volume of ballast, both in solid elements. A dynamic load was applied vertically on top of the sleeper to simulate the passing of a double axle bogie. Linear elastic springs were fixed on top of the sleeper to represent force of the rail pulling the sleeper back to its initial place.

In order to analyse the effect of hanging sleepers, interface elements were used in between the ballast and the sleeper to simulate hanging gaps. The idea is that these elements transfer no stresses when the surfaces are physically separated, and adopt Mohr-Coulomb criteria as soon as the surfaces approach each other. This method turned out to be very difficult to implement, despite numerous discussion with the software engineer it was not possible to script this in the FE software in such a way that all calculations converged without any errors.

During the modelling of the sleeper, it was found that the forces on the sleeper are highly dependent on the resistance of the rail. The rails have such a high bending stiffness that they hardly show any curvature over the length of only a few meters, so the sag of the rail is mainly dependent on the behavior of the surrounding sleepers. It was concluded that, to get a good picture of the behaviour, it is not sufficient to model only one individual sleeper, but it is necessary to look at a larger part of the railway track in order to involve the coupling between the sleepers.

The results from the computational model were used to determine the magnitude range and the frequency domain of the values to be measured, in order to be able to select the right measuring instruments. The results were also used to select the right positions for the sensors on the sleeper. Due to the constraints described above, a certain margin of uncertainty has been adopted.

The vertical speed of the sleeper is best measured with accelerometers, the large amount of previous applications of this type of measurement has shown that this measurement works well and will not lead to problems.

It was considered to use pressure cells for the measurement of interface stresses, though this device turned out to be difficult to fix at the sleeper and it gives very little information on the distribution of stresses. It was concluded that the best way to measure the ballast-sleeper interface stresses is by using the matrix based tensile surface sensor (MBTSS). This instrument is able to capture the stress distribution on a surface over time, by measuring the electrical current flow through a matrix of conductive lines, the current is resisted when certain forces are applied on the surface. Tekscan is a manufacturer that offers a wide range of MBTSS types, including sensors previously used in railway measurements. A certain protection will be needed to protect the sensor from being damaged by the ballast particles.

Previous applications of MBTSS in railway structures showed the calibration of the sensor to be very difficult. This presumably has to do with the way the stresses are distributed over the sensor surface. Since the stresses of the ballast are often compressed to very small contact points, it should be made sure the stresses will not get lost between the sensels, that are the points on the surface where the stress magnitudes are measured. The advice is to cover the MBTSS with an under sleeper pad, this is a relatively stiff mat that, in addition to offering protection to the sensors, also spreads the ballast forces. Laboratory tests will have to be performed in advance of the field measurement to test whether a correct calibration is possible. It can not be made sure that a fully successful calibration method will be found and therefore additional measurements are recommended for a validation for the stress magnitudes.

A first validation can be found by equating the sum of the vertical forces with the mass times the acceleration of the sleeper. To find the sum of the vertical forces, the load on top of the sleeper at the rail-sleeper connection, has to be measured as well. This can be realized by placing MBTSS between the baseplate of the rail and the sleeper. Similar measurements described in literature proved this type of measurement to be feasible. Furthermore, the result of the acceleration measurement will have to be used here as well.

A second validation can be performed by determining the moment distribution over the length of the sleeper, this can be conformed to the magnitude and distribution of the vertical stresses on the sleeper. The most reliable way to perform this validation is by using fiber measurements to find the moment distribution over the whole of the length. The most important positions over the length of the sleeper are under the rails and in the middle of the sleeper, because the peaks in the moment distribution are expected here based on the computational model calculations.

# PREFACE

This report is the result of the research performed as the final part of the master degree Structural Engineering at the Delft University of Technology. The circumstances under which this thesis was written were different from what I had expected due to the pandemic, with a lot of digital meetings and mainly working from home, which proved to be an extra challenge. Nevertheless I look back at this period with a positive mind because of the great deal of experiences and the tremendous amount of knowledge I gained. Due to the subject of my research, I have learned a lot about the fields of computational modeling, applied dynamics, railway engineering and field measurements, some of which were not or hardly treated during the rest of my masters.

This thesis was conducted in collaboration with Deltares, I would like to express my gratitude to this company for the fascinating topic they offered and for the facilities and possibilities they provided, it taught me a lot about the world of the scientific researches. In particular I would like to thank Paul Hölcher for the extensive and sincere support he offered during the process based on his profound knowledge and vast experience, I have enjoyed the many conversations, discussions and lectures that took place during our weekly meetings. Furthermore I also want to thank Vahid Galavi for his guidance in computational modelling and Avni Jain and professor van Dalen for their feedback on my report. Finally it want to give thanks to my friends, my family and my girlfriend for their words of encouragement and for their mental support along the way.

*Remco Bolhuis  
Delft, July 2021*



# 1

## INTRODUCTION

### BACKGROUND

The Dutch railway network is always subject to maintenance, which is disadvantageous for the financial costs for the railway infrastructure as well as for its inconvenience for train passengers and the reputational damage for railway operators. These maintenances often have to do with settlement of the tracks induced by the train loads. Section of a railway track that require more maintenance in particular are transition zones, which are the sections where the track structure changes from a ballasted trackbed on a soil embankment to a more rigid substructure, e.g. a concrete slab at a bridge or tunnel. The change in stiffness of the track structure is an important cause of differential settlements, of which the deteriorated track geometry will subsequently increase the deterioration process itself.

Despite the large amount of researches on mitigation measures in the past decades, it is still difficult to predict the behaviour of railway settlement in transition zones. Researchers often strive to clarify the stress distribution of the railway structures as precise as possible in order to get a clear understanding of the way deformations develop. They use computational models, for example finite element models, to explain the stress distribution and to predict the result of certain resolutions. A difficult part of the modelling is the validation, i.e. checking if the model is a correct representation of the actual situation. Validation of the model can be executed by physical measurements. The aim of the research described in this report is to find the best way to equip a railway sleeper with measuring instruments in order to perform such a measurement. This *measurement sleeper* should be able to measure the vertical contact stresses at the ballast-sleeper interface as well as its vertical velocity over time.

The first measurement, that of the interface stresses, is the most interesting because it allows for analyzing the forces on the ballast in combination with the compaction of the ballast, which is important because ballast compaction is often a cause for degradation

of the geometry of the railway structure. The focus of this research will mainly be on this measurement because there is little experience in this area. Developing a suitable measuring method for this could contribute to the decrease of railway maintenance, resulting in lower financial costs and less inconvenience for passengers. If this type of measurement turns out to work well, it could further be developed for the purpose of monitoring track behaviour in transition zones, this is however not within the scope of this research. The second measurement, that of the velocity, is important because the combination of the two greatly increases the reliability of the validation.

## ORGANIZATION

An NWO-funded project named “Rapid degradation of railway tracks on soft soils explained and mitigated: multi-scale dynamics modelling, a novel approach” was initiated and started by the TU Delft in 2018. Deltares is one of the users of this project, together with ProRail, Movares and Tensar. The aim of the project is to develop modelling software that can be used widely to reduce railway track maintenance costs through improved analysis and design of transition zones. The project studies the behavior of the ballast and subballast in railways and might use field measurements for the validation of the models, for which Deltares develops a measurement sleeper. The research described in this report is conducted in direct collaboration with Deltares and presents the design for this measurement sleeper.

## STATE OF THE ART

In recent decades, several measurements have been conducted on railway sleepers, mostly with the aim of reducing wear and extending the service life of the sleeper. In order to find out which measurement methods are suitable for the design of the measurement sleeper, an overview has been made of the precedent measurements regarding acceleration, strains and stresses on a sleeper.

Accelerometers are widely used instruments in railway measurements, they are relatively easy to use and provide information about acceleration as well as velocity and displacement, although mainly displacement data loses a lot of reliability due to the integration (Coelho, 2011; Rose et al., 2015; Paixao et al., 2018).

Also strain measurements have been performed on railways, usually with strain gauges but nowadays also by means of fiber sensors (Ngamkhanong et al., 2018). Strain measurements can be used to derive the bending moment over the length of the sleeper by mounting strain sensors on the sleeper (Edwards et al., 2017) or casting them inside the sleeper (Tran et al., 2020), but they have also been used to derive the magnitude of the train load on the rail (Coelho, 2011) or the load transferred to the sleeper (Gao et al., 2017).

A possible instrument for measuring the normal stresses at the ballast-sleeper interface are the pressure cells. Experiments have been performed both in the laboratory tests and in the field on the use of pressure cells to at the sleeper soffit (Stith, 2005; Rapp et

---

al., 2012), but this method provides little information about the distribution of the forces.

Another instrument for measuring interface stresses is the matrix based tactile surface sensor (MBTSS). McHenry (2013) investigated the applicability of MBTSS for dynamic ballast-sleeper interface measurements. The MBTSS comprises a matrix of electrically conductive lines and uses its change of conductivity when a pressure is applied on the surface to measure the magnitude of this stresses. McHenry concluded the method to be suitable for this type of railway measurements, though some questions remained about damage protection and calibration of the sensors. Gräbe et al. (2016) successfully used MBTSS for measurements on the ballast-sleeper interface in laboratory tests, but no literature was found on the details of this measurement. During this research it was discovered that Getzner Werkstoffe GmbH successfully developed a *sensor sleeper* which uses a measurement method similar to MBTSS to measure the ballast-sleeper interface stresses, however they were not open to share any information about this. Due to the successful findings for MBTSS in railway measurements, the focus in the design of the measurement sleeper will mainly be on this measurement method.

## REPORT STRUCTURE

This report will start with a literature study on the relevant aspects of railway structures in chapter 2. Subsequently, in chapter 3 the product requirements of the measurement sleeper will be laid down and explained. Chapter 4 will give a description of the computational model of a railway sleeper that is build for this research and it will present the outcomes of its calculations. Chapter 5 gives an overview of suitable measurement tools for this application. Chapter 6 will explain and argue the design of the measurement sleeper and chapter 7 will eventually explain how the calculations of the model are used to select the appropriate instruments for the measurement sleeper.



# 2

## RELEVANT RAILWAY FEATURES

This chapter will give an explanation of the features and the behaviour of a railway structure, in order to get a better understanding of the behaviour of a sleeper. The purpose of this is to be able to determine what points of attention there are in the design of the measurement sleeper and to be able to set up the product requirements. The first section of the chapter will give a description of the build-up of a transition zone and describe all components of the railway structure. After that, the features of the train loads on the sleeper will be given. Thirdly the behaviour of the sleeper, that is its displacements and deformations during commissioning, will be explained. Fourthly information will be given about the ballast layer, that is the settlement behaviour and the contact points at the ballast-sleeper interface. The fifth section will describe the remaining mechanisms in the railway structure. Finally, conclusions will be drawn that are important for the design of the measurement sleeper.

Since the actual location of the monitoring project is not known, the design for the measurement sleeper is in principle generic and applicable to any transition zone in the Dutch railway network. For the sake of thoroughness and completeness of this study, it is decided to choose one particular location as an example in order to use its representative characteristics for the design. The selected location is a transition zone close to railway station Gouda Goverwelle, from here referred to as location Goverwelle. Arguments for the choice of this location are the fact that it is a representative Dutch transition zone and it is in the past subjected to several researches, which makes it easy to find information on the current state of the transition zone.

### 2.1. RAILWAY ELEMENTS

#### 2.1.1. TRANSITION ZONE GOVERWELLE

The test site of location Goverwelle is located just outside the eastern residential areas of Gouda at the railway track in the direction of Utrecht, as shown in figure 2.1. The tracks

are straight up to 500 meter eastwards where a gentle curve starts. Several diverging tracks are present in the vicinity of the transition zone. The original double-track railway was constructed in 1855 as a Gouda-Utrecht connection and was widened to a four-track railway around 1995. Deltares took part in an extensive field test on location Goverwelle in 2008. The information in this section is largely based on findings in that research, mostly via Hölscher and Meijers (2009) and Coelho (2011).



Figure 2.1: Location test site (Google Earth)

The stiffness transition in the railway structure at location Goverwelle is caused by the crossing of a watercourse through a culvert construction. The concrete culvert has a width of 2.150 meter and is founded on piles. Approach slabs of reinforced concrete with a thickness of 0.3 meter and a length of 4 meter are hinged to the top corners of the culvert with the purpose of mitigating the effect of the sudden transition. A ballast layer is present in the railway track throughout the crossing of the culvert. The culvert does not show any significant displacements on both long- and short-term and can thus be considered as a fixed point.

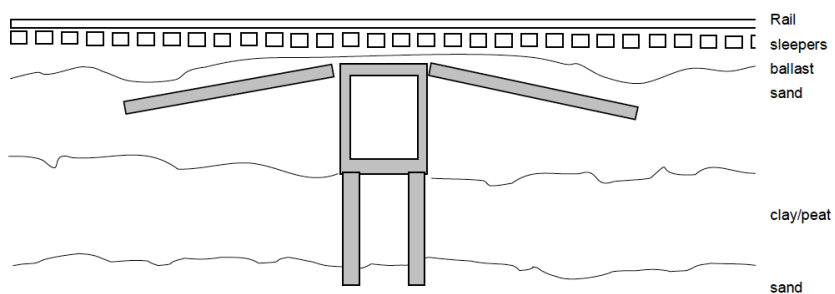


Figure 2.2: Schematic view of culvert construction with approach slabs (from Hölscher and Meijers, 2009)

### 2.1.2. SLEEPER

Wooden sleepers have been used at location Goverwelle, however nowadays concrete sleepers are applied in all new railways by Prorail. Concrete sleepers are less elastic,

have a longer life and have a larger mass which makes them somewhat more stable. The most common sleeper is the NS90 type, though in special cases (e.g. transition zones, small curve radii, railway turnouts) the 14-002 sleeper is used instead, a top view of the latter is shown in figure 2.3. The sleeper has a height of 0.3 meter and a mass of 369 kg. The sleepers are applied at a centre-to-centre distance of 0.6 meter. ProRail laid down regulations for the admission of railway sleepers (E. Gerlinck, personal communication, February 2, 2020).

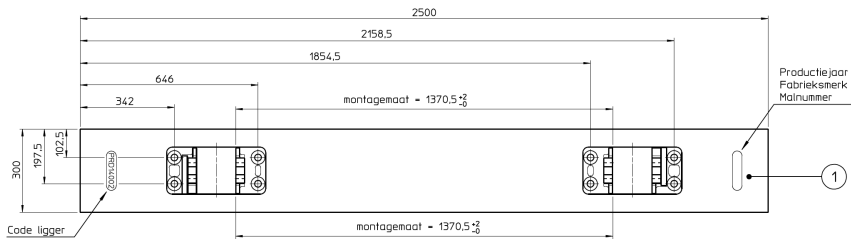


Figure 2.3: Top view of concrete railway sleeper 14-002 (ProRail productnumber PRD14002)

### 2.1.3. RAILS

The used rail profile at location Goverwelle is, as it is in all standard Dutch railway tracks, the so called flat-bottom rail. Almost all Dutch railways makes use of the 54E1 profile, having a total height of 159 mm and a standard gauge of 1435 mm. Fastening systems are used to connect the rails to the railway sleepers. The rails are subjected to wear and therefor have to be replaced after a certain time, but this has no relation with ballast compaction and is therefore not within the scope of this research.

The rails are also used to conduct electricity. Almost all trains in the Netherlands use electric traction, and allow a direct current of 1500V to flow via the overhead line to the train, and via the steel wheels to the rails (*retourstroom*) back to the feeder station. Apart from this an alternating current is used in the rails to constitute a track circuit that will be short out by the wheels when a train passes, this makes for a relatively simple and reliable detection of trains.

### 2.1.4. FASTENING SYSTEM

In the connection of rails on concrete sleepers, the rails are placed on rail baseplates which are each fastened with four bolts to the sleeper. The rails are placed in the slot of the baseplate and held in place by clamps which are bolted through the baseplate to the sleeper. A rubber railpad is placed underneath both the baseplate and the rail to provide mitigation of the dynamic loading and reduce the stressing and fatigue loading on the sleepers.

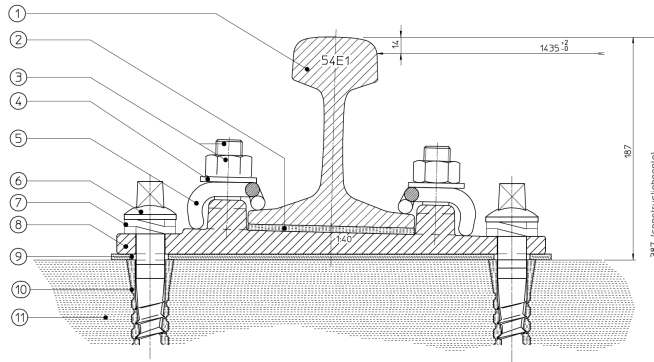


Figure 2.4: Detail rail-sleeper connection, 1; rail profile, 2; railpad, 3; clip bolt, 4; washer, 5; sleeper clip, 6; collar bolt, 7; double spring washer, 8; baseplate, 9; cork-rubber baseplate pad, 10; screw sleeve, 11; concrete sleeper (E. Gerlinck, personal communication, December 23, 2020)

### 2.1.5. BALLAST

The ballast layer underneath the sleepers comprise crushed stone with typically a 31.5 to 50 mm grading. The ballast is packed around the sleeper to ensure lateral stability. Literature often describes a finer graded subballast layer at the bottom of the ballast, but this layer was not distinguished in any of the researches at location Goverwelle. There is no clear boundary between the ballast layer and the sand embankment as initially designed due to the irregular compaction and mixing of the ballast layer, caused by the many train passages and re-tamping and re-ballasting in the past decades. The thickness of the ballast layer varies from approximately 0.5 meter close to the culvert up to 1.2 meter near the toe of the approach slab. The ballast behaviour will be further described in section 2.4.

### 2.1.6. SUBGRADE AND SUBSOIL

The ballast layer at location Goverwelle is rested on a subgrade of sand. Though the mixing of ballast and sand is not studied in detail in this case, it can be assumed that some mixing has taken place. A mixed zone of about 0.2 meter seems possible (Hölscher and Meijers, 2009). The depth of the lower boundary of the sand layer varies from approximately 4 to 6,5 meter measured from the sleeper soffit. Below is a peat layer with a thickness of 3.5 to 5 meter present, with a sand layer of varying thickness within.

## 2.2. TRAIN LOAD

### 2.2.1. VERTICAL FORCES

The main train load will be transferred as a vertical load upon the rails. Train carriages usually have two bogies with each two axles. In the monitoring project at location Goverwelle in 2008 were the magnitude of the axle loads measured by means of train gauges mounted on the rails (Coelho, 2011), the findings of this measurement are showed in table 2.1. The American Railway Engineering and Maintenance-of-Way Association (AREMA) Manual for Railway Engineering presents information about the wheel-to-rail load car-

ried by an individual sleeper and shows that for a 0.6 m centre-to-centre sleeper spacing up to 50% of the load is carried by one sleeper. The dutch rail network permits an axle load up to 225 kN. The maximum service speed of dutch trains is 140 km/h, measurements at location Goverwelle found a speed range of 65 to 130 km/h.

Train	Axle load [kN]	Distance wheels [m]	Distance axles [m]	Length [m]
Intercity double deck (IDD)	127-193	2.75	20	28.2
Intercity single deck (ICM)	97-143	2.5	19	27.05
Intercity locomotive (ILC)	160-215	2.8	9.7	17.9
Local train (Mat V)	96-136	2.75	14.35	24.93
Sprinter	77-124	2.5	18.1	26.1

Table 2.1: Train load description (from Coelho, 2011)

Vehicle- or rail defects might induce vertical forces as well, however these are not mentioned in literature on location Goverwelle and are therefore not within the scope of this project. Rolling of the vehicle might also lead to vertical forces, this might be relevant in a transition zone because of the level fluctuations of the rails. Also, the load might be uneven distributed over the rails because of curves or asymmetries in the railway structure or the train. Uneven settlement of the ballast and the soil allow for this phenomenon to amplify itself.

### 2.2.2. LATERAL FORCES

Lateral forces, that is horizontal forces perpendicular to the track direction, occur as a result of turnings in the railway. These forces are not significant in location Goverwelle because it has no curvatures nearby, but it might be relevant for different locations. Lateral forces can also occur because of hunting oscillations; the thread of the wheels is slightly tapered wherefore the wheelset usually stays in the centre of the rails and the flanges make no contact with the rails, but the additional space between these flanges might lead to lateral motions. Other types of yawing and rolling of the vehicle might also lead to lateral forces. The influence of these effects are dependent on the situation and its contribution to vertical force distribution is usually of a small order of magnitude, so it is not studied more profoundly in this research.

### 2.2.3. LONGITUDINAL FORCES

Longitudinal forces can occur as a result of temperature changes, acceleration and braking of the train, shrinkage and creep. The development of axial forces is largely prevented by means of joints which allow for length changes of the rails and does not have significant influence on the sleeper, therefore it is not further elaborated in this study.

## 2.3. BEHAVIOUR SLEEPER

This section gives an overview of all possible displacements and deformations of the sleeper and their probability and relevance for this research. Vertical movements, hori-

zontal movements and deformations are treated separately in the next subsections. Within these sections is made a division between short-term effects and long-term effects if necessary. Short-term refers to the behaviour during a train passage, long-term effects refer to plastic deformations in the railway structure.

### 2.3.1. VERTICAL DISPLACEMENT

#### TRANSLATION (SAG)

The vertical translation is the most evident movement of the sleepers during the passage of a train. The magnitude of short-term movements, that is the short vertical displacement when a train axle crosses a sleeper, depends largely on the ballast support underneath the sleeper. An increasing hanging distance provides room for larger displacements and will presumably also increase the length of the influence range of the load. The vertical displacement time history of a sleeper for a train passage close to the culvert found by Coelho (2011) is shown in figure 2.5. Note that the graph does not give absolute values because the graph is somewhat ‘shifted upwards’ in the middle due to incorrect adjustment of the numerical integration.

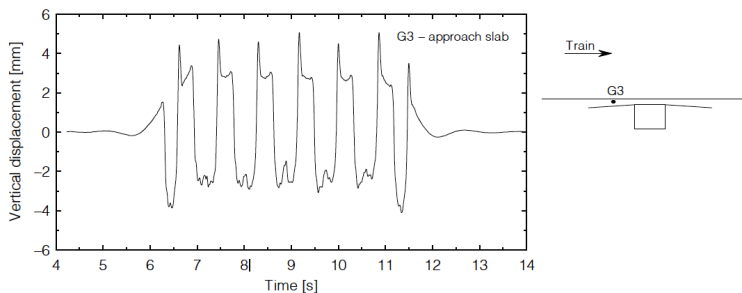


Figure 2.5: Vertical sleeper displacement during passage of a train at 114 km/h (Coelho, 2011)

Long term sag of sleepers is the result of ballast settlement, which is treated more profoundly in section 2.4. The sleepers will sag along with the ballast, for as far as they are not retained by the rails because of height differences of surrounding sleepers. Differential sag of the sleepers creates hanging distances resulting in higher dynamic loads, so the short-term and long-term displacements are interdependent. Figure 2.6 shows how the rails, and thus the sleepers, settle with respect to the the initial situation directly after tamping at location Goverwelle. The graph confirms that the track will barely settle at the location of the culvert structure, that is at sleeper 29 on the x-axis. It also shows the track settles 14 to 16 mm from a couple of meters away from the structure. The differences in settlement on both sides of the culvert might be due to the driving direction of the train or due to differences in the subsoil.

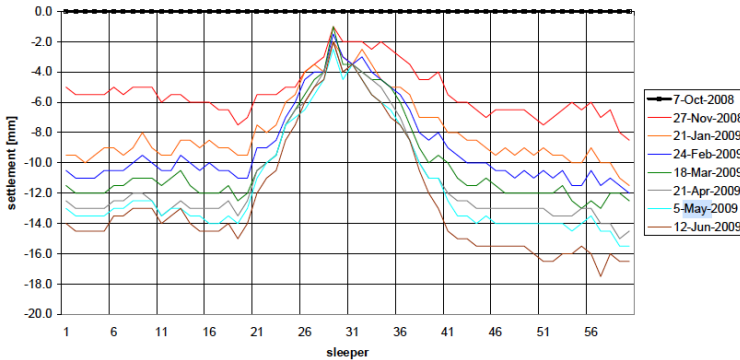


Figure 2.6: Settlement at top of rail at transition zone at location Goverwelle (from Hölscher and Meijers, 2009)

### LATERAL ROTATION (CANT)

An uneven settlement over the length of the sleeper will cause a lateral rotation, also called cant. The irregularity of the soil and ballast particles and in some cases the asymmetry of the railway structure and the train loads make a uniform settlement of the sleeper in practice unlikely so some cant will be inevitable. The interaction between the sleeper movements and ballast settlement might amplify this process. The situation for a single sleeper can therefore not be addressed as a symmetric problem. At location Goverwelle was found that the level of the outer rail, that is the rail closest to the ballast slope, is always a tad lower than the level of the inner rail due to smaller confining pressure and flow of ballast towards the outside. The level difference is of an order of magnitude of 1 mm.

### LONGITUDINAL ROTATION

Uneven sag in the track direction, so the width of the sleeper, would lead to a rotation of the sleeper in the longitudinal direction of the track. The orientation of the sleeper with respect to the rails makes this motion unlikely and not of relevance in the degradation process of the track. No literature was found on this motion of railway sleepers.

## 2.3.2. HORIZONTAL DISPLACEMENT

### LATERAL TRANSLATION

Since lateral forces, that is horizontal forces perpendicular to the track direction, can occur in railways, in particular near railway curves, it is also possible for sleepers to translate in a lateral direction. This movement might let the sleeper slowly 'dig in' the ballast layer and thereby lead to track settlement. Literature on the monitoring project at location Goverwelle does not mention horizontal movements of the sleeper, but it was mentioned that the values for horizontal movements in the embankment were too small to give reliable numbers, meaning the displacements are less than 2.5 mm per year.

### LONGITUDINAL TRANSLATION/ROTATION

Horizontal forces in longitudinal direction of the track can theoretically lead to a backward or forward shift of the sleeper. Unequal longitudinal forces of the rails might lead

to a rotation of the sleeper. The stiffness of the rails in longitudinal direction makes these movements unlikely and no literature is found on this type of sleeper movements.

### 2.3.3. DEFORMATION

#### BENDING

The loads on top of the sleeper are applied at the location of the railseats and the ballast at the bottom of the sleeper might be uneven distributed, so a varying moment distribution will arise over the length of the beam. According to Edwards et al. (2017) the bending moment would reach a maximum in the centre with a magnitude up to an order of magnitude of 25 kNm for heavy-haul freights. This moment comes with a proportional bending which can be derived directly from the bending moment using the stiffness properties of the sleeper.

## 2.4. BEHAVIOUR BALLAST

### 2.4.1. SETTLEMENT

Track settlement is the result of an accumulation of thousands of very small non-elastic deformations of the ballast, and to a lesser extent the subgrade, caused by each train passage. This deformations come mainly in the form of densification. The causes of the densification of ballast and subgrade can be attributed to the mechanisms listed below (Dahlberg, 2004).

1. Volume reduction will, particularly in the first phase, be caused by particle rearrangement produced by the repeated train loading.
2. The subgrade will penetrate into the ballast voids, which causes the ballast to sink into the subgrade.
3. Particle breakdown, that is fracture of the ballast particles, can be caused by train loading and environmental factors and lead to volume reduction.
4. Abrasive wear will happen in particular at the contact points with other ballast particles and thereby lead to a volume reduction.

Aside from densification, the mechanisms listed below give rise to the settlement of the ballast and subgrade as well.

1. Due to micro-slip between ballast particles at loading, all deformations will not be fully recovered upon unloading the track, leading to permanent deformation.
2. Particles move away from under the sleeper, causing the sleeper to sink into the ballast.
3. Lateral and possibly longitudinal movements of the sleeper cause the ballast particles beneath the sleeper to be pushed away and make the sleeper sink deeper into the ballast.

After tamping maintenance the settlement starts directly with a relatively high speed. In this phase the gaps between the ballast particles reduce and the ballast becomes consolidated. Later on the settlement takes on a much slower and more or less linear pace,

which seems in a greater extent caused by settlement of the subsoil. The graph in figure 2.7 confirms this process. The nature of these mechanisms make predicting the course of the settlement behaviour of ballast the main difficulty in the modelling of the railway structure.

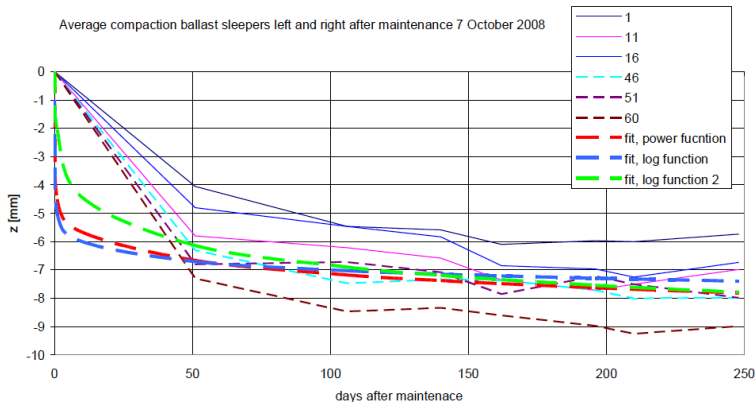


Figure 2.7: Densification ballast at location Goverwelle after tamping (from Hölscher and Meijers, 2009)

### 2.4.2. CONTACT POINTS

The distribution of contact points of the ballast on the sleeper is studied by Abadi et al. (2015) using pressure paper that turns red when a pressure within the range of 10 to 50 MPa is applied. One of the laboratory test in this study comprised the application of 3 million load cycles on a concrete sleeper with similar dimension, supported by a similar ballast grading as present at location Goverwelle. Manual reading of the paper learnt that the contact area of the ballast was 0.18 percent of the bottom surface, distributed over 147 contact points. This corresponds with an average contact pressure of 76.5 MPa. It can be seen that the contact is most pronounced beneath the railseats. Note the distribution of the contact points is very dependent on the material of the sleeper and whether or not an under sleeper pad is placed underneath the sleeper.

## 2.5. OTHER MECHANISMS

### 2.5.1. HANGING SLEEPER

As a result of the ballast settlement near the stiff structure in a transition zone, the sleeper will lose contact with the ballast layer and start to hang on the rails, this phenomenon is referred to as hanging sleepers. At location Goverwelle the sleepers on top of the culvert do not show any loss of contact with the ballast, but the sleepers directly next to the culvert show a relatively large hanging distance. The dynamic stresses on the sleepers increase because of this hanging distance, which amplifies the degradation process itself at the transition zone. The research from Coelho (2011) made use of Vortok hanging sleeper devices to give an estimate of the hanging distances, the results of this measurement are showed in figure 2.8. Though the accuracy of the Vortok devices is poor, it does give a useful qualitative assessment of the sleeper gaps. The differences in settlement on

both sides might very well be the result of the direction at which the trains pass the culvert, though the driving direction was not given with this graph. The asymmetry of the graph might also be explained by differences in ballast composition, soil composition, geometry of the structure or by the relatively large measuring uncertainties.

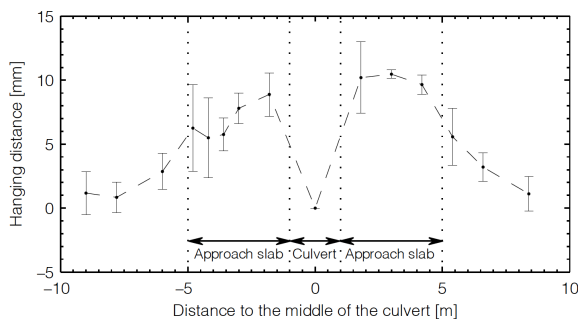


Figure 2.8: Estimation of hanging sleeper distance at location Goverwelle during end of maintenance cycle (from Coelho, 2011)

### 2.5.2. FAILURE MECHANISMS SLEEPER

According to Edwards et al. (2017) the most common factors limiting the service life of prestressed concrete sleepers in North America is central cracking, followed by rail seat cracking. Ferdous and Malano (2014) studied a wider range of degradation mechanisms for sleepers. They emphasized failure by cracking because of tensile stresses in the concrete, mainly as a result of wheel- or rail abnormalities. Tamping is also mentioned as an important cause for damage, along with chemical causes, such as delayed ettringite formation, alkali-aggregate reactions, acid attacks, ice forming and bar corrosion. These mechanisms are however not the focus of this research and the measuring equipment will presumably not be of influence on these mechanisms.

### 2.5.3. FAILURE MECHANISMS SUBGRADE

Since the railway track is usually located on an elevation of the soil, the most important failure mechanism of the subsoil is sliding of the soil structure of the railway on a macroscale, including the ballast layer and sleepers, although this depends on the specific railway construction. Sliding can also happen on a smaller scale, so that only the ballast layer will fail. There is little relation between these mechanisms and the behaviour of a sleeper, so this topic has not been further explored.

## 2.6. CONCLUSION

When considering a sleeper in a dutch transition zone, one should focus on the 14-002 type concrete sleeper. The sleeper is subjected to axle loads up to 225 kN with a maximum train speed of 140 km/h. The stresses are transferred to the sleeper soffit via very small contact points due to the geometry of the ballast particles. The train load is mainly transferred in vertical direction, so the vertical displacement of the sleeper is most im-

portant for this design-study. Note that curves and asymmetries of the track might allow for an uneven load distribution over the rails, so rotation of the sleeper should be taken into account as well. Lateral and longitudinal forces may also occur, but the influence of this on sleeper displacements is small, therefore horizontal movements will be disregarded in this study.

Compaction of the ballast will lead to a relatively fast settlement in the first phase directly after tamping maintenance, after this the structure will show a slower, stable settlement, presumably on account of the subsoil, until new maintenance takes place. In transition zones this settlement will lead to hanging distances within approximately five meters of the stiffness transitions. Field measurements at location Goverwelle showed that the hanging gaps developed heights up to about 11 mm. Failure mechanisms of the sleeper and the subgrade are not of frequent occurrence and are not regarded in this study.



# 3

## PRODUCT REQUIREMENTS

As mentioned, the purpose of the measurement sleeper is to take measurements for the validation of computational models. This chapter will lay down in more detail what measurements are wanted and what requirements are assigned to these measurements in order to achieve this goal. Later on in the chapter, further requirements for the beam and possible risks of the design will be mentioned. It goes without saying that recording these requirements is necessary in order to be able to develop a good design.

### 3.1. MEASUREMENTS

#### NORMAL STRESSES

The first main requirement of the design is to measure the normal stresses at the ballast-sleeper interface, that are the vertical stresses transferred from the ballast particles to the sleeper soffit. If the primary measurement is not able to give sufficiently reliable data to use it for validation, additional measurements can be used to validate the magnitude of the stresses. As explained in section 2.4.2 the stresses are compacted to small contact points. Since it might not be feasible to measure the stress peaks at the contact points exactly, it is required to measure the distribution of the stresses as detailed as possible with the available measuring equipment.

#### VELOCITY

The second main requirement is the measurement of vertical velocity of the sleeper, since the combination of this and the aforementioned measurement allows a solid validation of a computational model. Velocity of the sleeper might variate over the length of the sleeper due to deformations, though the design should make it possible to acquire the average velocity over the length of the sleeper.

#### ACCURACY

The measurements of the sleeper should capture the effect of the passing of a train as accurate as possible. Section 2.2 describes what the train load will look like and the velocity

of it's passing. Calculations of the computational model will give a more profound approximation of the expected stresses. The measuring instrument should be able to capture the course of the stresses at all train speeds that can reasonably occur and should thus feature a sufficiently high measuring frequency.

#### DURATION

It is desirable for the monitoring of long term effects to capture the whole of a maintenance cycle, this takes approximately a year. This time span is also reasonable from an executive perspective. The measuring sleeper must therefore be serviceable for a period of at least one full year.

### 3.2. DEMANDS SLEEPER

#### ADMISSION

Since the sleeper must be allowed to be installed in an existing track, it must agree with the requirements for existing sleepers. It must be made sure the measuring equipment will not affect any features contributing to the main purpose of the sleeper itself. Since a full admission test would take too much time, the measurement sleeper should agree with the guidelines laid down by ProRail. The following functional requirements are assigned to the sleeper (SPC00094, section 2.1);

1. offer support- and mounting options for rails and turnouts of the 54E1/E5 and 60E1/E2 profile;
2. take on stresses on the rails as a result from train passages and temperature and distribute them as good as possible over the ballast layer;
3. guarantee the horizontal geometry of a turnout and track gauge;
4. guarantee the slope of the rail profile;
5. provide sufficient electrical insulation to the rail profiles;
6. resist mechanical impacts and environment influences.

ProRail has elaborated this into many performance requirements, e.g. sleepers with a centre-to-centre distance of 0.6 meter on a ballasted track should be able to resist axle loads of 25 tonnes at a speed of 120 km/h. Admission will eventually have to be granted by ProRail, so it might be useful to consult ProRail during the design process when doubts arise, in order to prevent wasting time because of inadmissible choices. A demand worth mentioning is that problems concerning the track circuit caused by the measuring instruments, such as stray current, short circuit or EMC, must be avoided. Furthermore it is only possible to drill in the sleeper for the mounting of instrumentation within the appointed drilling zones, to make sure the reinforcement won't be affected. Special adjustment to the concrete might be possible in cooperation with the manufacturer.

#### NON-INVASIVE

It is essential for the design that the measurements will not be affected by the measuring equipment itself. In other words, the tools and the way they are mounted to the sleeper

should not change the properties that influence the stress distribution on the sleeper. This holds for the following properties of the sleeper:

1. shape and moment of inertia
2. mass
3. surface roughness
4. stiffness

It should be made sure in the design that these properties will not be affected or otherwise the effects should have no significant influence on the measurements.

### 3.3. RISKS

#### ENVIRONMENT

The following risks can be distinguished as due to influences of the environment:

1. Temperature changes; the instrumented sleeper should be able to resist very high temperatures in the sun as well as frost in the winter.
2. Moisture; the sleeper will be exposed to water, in particular from the rainfall.
3. Chemical effects (e.g. corrosion); the moisture, acid or other environmental substances might give rise to chemical reactions.
4. Plants and animals; although ballast is not an attractive place for plant growth and animals to settle, it cannot be ruled out that either of them might affect the sleeper.

#### MEASUREMENTS

The correctness of the measurements might be sensitive to the following risks:

1. Fixation of the measuring instruments can be incorrectly or insufficiently, or they can be placed at the wrong position.
2. Measured values can be too low for a particular instrument, meaning it is not able to give reliable measurements.
3. Measured values can be too high, meaning it will give unreliable measurements or even damage the instrument.
4. Malfunction, too low a quality or otherwise failure mechanisms are possible specific for particular instruments.

#### DATA

The following risks might be at hand concerning the handling of the measured data:

1. Numerical integration, for example to deduce displacements from acceleration, will not be exact and might drift due to numerical mistakes.
2. Measuring instruments might need calibration, mistakes or shortages of these calibrations might give erroneous data.
3. Data can be affected by noise for several reasons, this depends on the measuring method and should thus be considered separately per instrument.



# 4

## COMPUTATIONAL MODEL

A 3D finite element model has been built for this research with the aim of approximating the behaviour of a sleeper. With this model the magnitude ranges and the frequency domains of the values that are to be measured with the measurement sleeper can be estimated, which is necessary to choose the right measuring instruments. The model comprises one single sleeper and adopts linear elastic material properties to keep it manageable within the relatively short amount of time allocated to this project. This simplifications require some important assumptions, which will be advocated in this chapter. The basic idea of the model will be explained in section 4.1.1. The different components of the model will each be clarified in sections 4.1.2 to 4.1.7. The end of the chapter will describe the conclusions drawn from the calculation.

For this research is made us of the open-source software Kratos, this software is written in C++ programming language and allows for a wide range of numerical methods for finite element calculations. As for any open-source software the user is not limited by any licences, which is a drawback for commercial software packages. Within Deltares there was the question of whether Kratos is a suitable software for wider application, which made the software interesting to use for this project. Support was offered by a software engineer from within Deltares. The disadvantage for this open-source software however is that it is less user-friendly and the help function is very limited. Specific calculations often required certain plug-ins and adjustments in the script, which gave rise to delay in this research.

### 4.1. MODEL FEATURES

#### 4.1.1. BASIC IDEA

The model comprises two bodies composed of solid elements, that is the sleeper and a volume of ballast, as shown in figure 4.1. The dynamic train load will be applied on top of the sleeper at the location of the rails, the resistance of the rail by 'pulling up' the sleeper is simulated by springs at the location of the bolts of the rail connection. In order

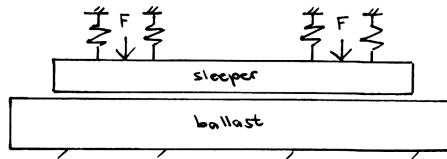


Figure 4.1: Build-up of the FE model

to make it possible to simulate the effect of hanging sleepers, special attention is given to the ballast-sleeper interface at the sleeper soffit. The calculation starts with a first phase in which the sleeper and the springs will be shifted upwards to create the hanging gap, this part of the calculation is quasi-static. In the second phase of the calculation the train load will be applied and the behaviour of the sleeper can be analyzed, this part of the calculation is dynamic.

#### 4.1.2. SLEEPER

The model is based on the 14-002 sleeper since this sleeper is typically used in transition zones as was explained in 2.1.2, the dimensions are depicted in figure 2.3. The sleeper is made of concrete with strength class C50/60 and is equipped with reinforcement en prestressing steel. Since the cross-section is constant over the length, it has been considered to model the sleeper in (2- or 3-node) beam elements as this will adequately lower the degrees of freedom and thus allow for smaller time steps and/or a more refined mesh. However, since solid elements would give additional information on the stress variations in the cross-sections and this was expected to be manageable in terms of computational effort, it was chosen to use solid elements. The elements are tetrahedron-shaped and are quadratic (10 nodes) to prevent shear locking problems.

It is expected no cracks will develop in the sleeper since it is prestressed and the concrete will remain in its linear elastic stage. The Young's Modulus of the concrete and the prestressing steel is respectively 37.3 and 200 kN/mm<sup>2</sup>, so the steel is approximately 5 times stiffer. The reinforcement steel will reasonably account for no more than 1% of the surface area of the cross section, which will increase the stiffness of the sleeper with only a factor 1.04. This influence is insignificant, it will be overruled already by the uncertainty margin of the adopted characteristic property values of the concrete. For this reason it is decided to exclude the reinforcement steel from the model.

The sleeper is equipped with prestressing steel to prevent the concrete from cracking. Image 4.2 gives an impression of the influence of the prestressing, assuming the concrete will remain in its linear elastic stage; it will only lead to an overall shift in longitudinal stress so that it will be all in compression. The purpose of this model is to study stiffness and not failure of the sleeper, since the stiffness is not affected by the prestress it is permitted to exclude the prestressing steel from the model as well.

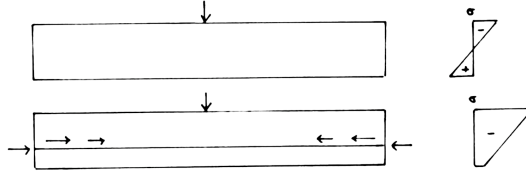


Figure 4.2: Diagram on influence of prestressing steel on the concrete sleeper

### 4.1.3. BALLAST

The plastic behaviour of ballast is very important for long term analysis of railway tracks, however the long term effect is included in the hanging distances in the models. The non-recoverable plastic deformation per single axle passage is generally several orders of magnitude lower than the resilient deformation (Varandas et al., 2020). Since each model only analyses separate passages of two-axle loads, the plastic behaviour is disregarded and the ballast element properties are elastic. The elements used for the ballast are 10 noded quadratic tetrahedrons.

#### STIFFNESS

When searching for a suitable value to simulate the ballast stiffness in a linear way, a value of 130 MPa is frequently used in literature (Varandas et al., 2020; Paixao et al., 2018). The stiffness behaviour of the ballast can be estimated with the following function (Varandas, 2013):

$$E_{nonlinear} = K_1 \left( \frac{\theta_t}{\theta_0} \right)^{K_2} > E_{min}$$

In his latest report Varandas recommended to use the values  $K_1 = 110$  MPa,  $K_2 = 0.6$  and  $E_{min} = 16$  MPa (Varandas et al., 2020). The reference stress ( $\theta_0$ ) is connected to the initial loading of the ballast, this is set to 100 kPa (Varandas, 2013). Now that the stiffness can be expressed as a function of the compressional stress on the ballast ( $\theta_t$ ) in kPa, as is shown in figure 4.3. In order to confine the complexity and computational effort of the calculation, the properties of the ballast elements in this model are linear elastic. First calculations showed that the stresses on the ballast-sleeper interface range up to 200 kPa with averages around 100 kPa, so the ballast stiffness is set to 100 MPa.

#### DIMENSIONS AND BOUNDARY CONDITIONS

The sleeper is surrounded by crib and shoulder ballast along its sides. It can be reasoned that these particles will transfer shear stresses to the sides of the sleeper which will influence the vertical motion. It is assumed that this influence will not be significant in the short term displacement of the sleeper because they will be relatively small, this is confirmed by Varandas et al. (2020). The crib and shoulder ballast is thus left out the model, only a volume of ballast underneath the sleeper is modelled.

The standard depth of ballast is 0.3 meter (Dahlberg, 2004) and is often divided from the subsoil by a layer of subballast, however findings from Coelho (2011) gave the impression

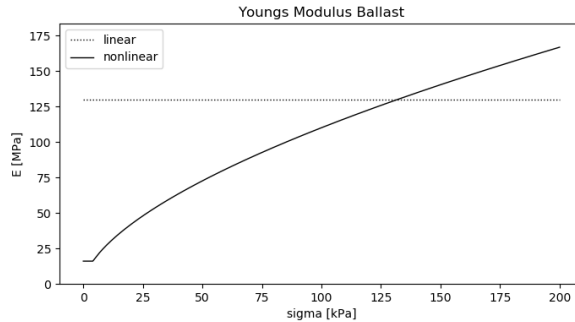


Figure 4.3: Nonlinear stiffness ballast according to Varandas (2013)

that the actual thickness of these layers is in practice not so clear because of intermixing and maintenance work during the lifetime of the track structure. The ballast volume in the model has a height of 0.3 meters and is fixed at the bottom, since it is assumed that the elasticity of the soil has no significant influence on the short term effects of a single train passage.

The width of the volume is set to 2.8 meters with no constraints assigned to the faces, since ballast can often move more or less freely on the side of a railway structure. These boundaries are thought to be the most general, knowing the actual boundaries at the sides are very dependent on the geometry of the particular track at hand. The ballast volume has a length of 0.6 meters in longitudinal track direction in accordance with the centre-to-centre distance of the sleepers. Since loads are always distributed over multiple sleepers, and adjacent sleepers are thus expected to show comparable behaviour, the surfaces perpendicular to the track are fixed in the track direction. Figure 4.4 shows the boundary conditions of the ballast in a side view of the sleeper model.

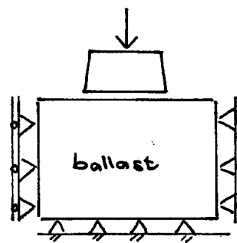


Figure 4.4: Side view showing the boundary conditions of the ballast body

#### 4.1.4. RAIL RESISTANCE

Apart from the train load and the ballast support the sleeper will be subjected to a third force, namely by the rails pulling the sleeper back at its initial state via the rail-sleeper connection. The magnitude of this resistance force is strongly dependent of the dis-

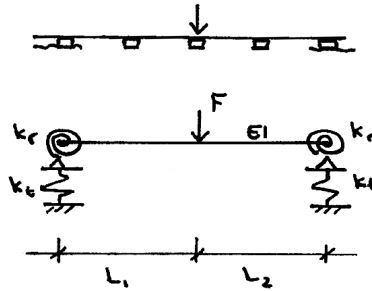


Figure 4.5: Euler-Bernoulli beam model used to determine spring stiffness for rail resistance

placement of adjacent sleepers and therefore highly nonlinear. Since the main parameter for the resistance force is the displacement of the sleeper, springs are used on top of the sleeper to simulate this rail resistance. Since a linear spring was used to keep the complexity of the model manageable, some rough assumptions must be made to be able to simulate the resistance of the rail. These choices and assumptions will be explained in this section.

To determine the magnitude of the rail resistance is made use of a static beam model as sketched in figure 4.5. The beam model depicts one or more adjacent hanging sleepers with a vertical point load applied to one of them, confined by two fixed sleepers at the outer ends. The vertical displacement ( $u$ ) of the beam model can be found by solving the fourth order differential equation known from structural mechanics ( $\frac{\partial^4 u(x)}{\partial x^4} = \frac{q}{EI}$ ) with the appropriate boundary conditions for  $x = 0$ ,  $x = L_1$  and  $x = L_1 + L_2$ . To express the force ( $F$ ) as a function of the displacement ( $u$ ), certain values are required for the rotational spring stiffness ( $k_r$ ) and translational spring stiffness ( $k_t$ ) at both sides, the bending stiffness of the beam ( $EI$ ) and the distances from the point load to the support on both sides ( $L_1, L_2$ ). The following subsections will explain how the values are chosen for each of these parameters.

#### ROTATIONAL SPRING STIFFNESS ( $k_r$ )

To determine the value for the rotational stiffness in the beam model, it is assumed that the rail will deform in a wavelike shape around the following sleepers, as sketched in figure 4.6. The rotational spring gives the moment at that point as a function of rotation, this value depends on the bending stiffness and the centre-to-centre distance of the sleepers and can be found using structural mechanics.

#### TRANSLATION SPRING STIFFNESS ( $k_t$ )

Note, as figure 4.5 shows, the translational spring  $k_t$  represents the support stiffness of the outside (not-hanging) sleeper, so it only partly influences the stiffness of the spring representing the eventual rail resistance. To determine the value of the spring stiffness is made use of the extensive dynamic analysis of the sleepers in the transition zone at location Goverwelle (Coelho, 2011). When adopting a displacement stiffness for supported

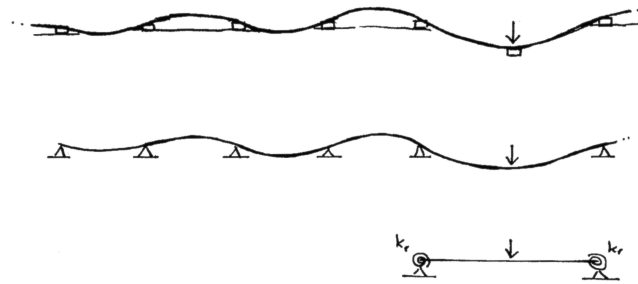


Figure 4.6: Diagram for rotational spring

sleepers in the beam model from the results of this measurements, the following issues might either overestimate, underestimate or over-simplify the stiffness value:

- The sleeper might ‘jump back’ when unloaded, leading to larger displacements (underestimation).
- Dynamic effects influence the displacement in reality, this might lead to larger forces than just the static axle load (underestimation).
- The measurements in the report are performed only halfway a maintenance cycle, hanging distance and thus vertical displacement might be larger later on in the cycle (overestimation).
- The axle load is based on generic properties for the train type, though the exact load might vary somewhat (uncertainty).
- The displacement of one sleeper is highly dependent of the displacement of surrounding sleepers, which makes the assumption of one stiffness value very plain (uncertainty).

It was concluded that an axle load of 160 kN led to a vertical sleeper displacement of 1.4 mm. Since maximal 50% of the axle load will be transferred to one single sleeper (further explained in 4.1.7) the load on the sleeper is 80 kN. From this the following value can be derived for the translational springs in the beam model:

$$k_t = F/u = 80000/0.0014 = 5.714 \times 10^7 [N/m]$$

#### BENDING STIFFNESS (EI)

The Young Modulus for steel is known to be 2.1 GPa and the moment of inertia of the common used 54E1 type rail (figure 4.7) is  $2.3379 \times 10^{-5} m^4$ . If this properties are used in the beam model, the fact that only one of the two rails is used can be compensated for by adopting only half of the load and spring stiffnesses when solving the beam equation.

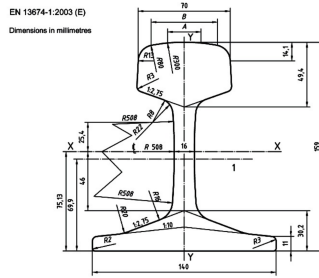


Figure 4.7: 54E1 Rail dimensions

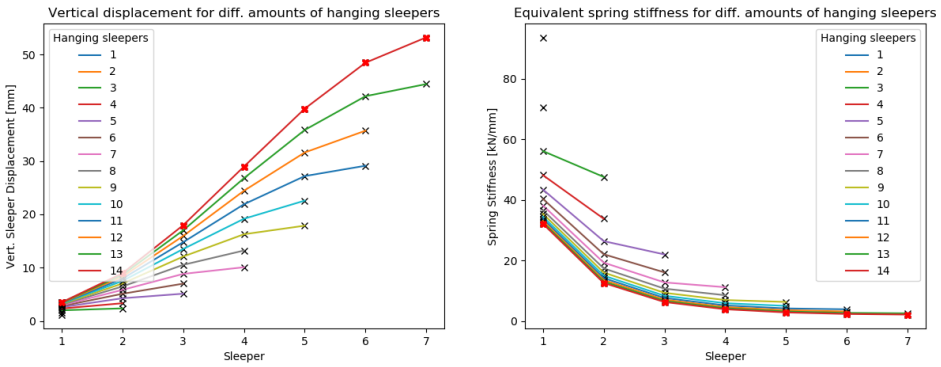


Figure 4.8: Deflection for 80 kN point load (left) and equivalent spring stiffness (right) for beam model with varying dimensions lengths

**SPAN ( $L_j$ )**

The final parameters to find an equivalent spring stiffness for the beam model are the span of the beam and the location of the point load, that is  $L_1$  and  $L_2$  in figure 4.5. Whereas an individual hanging sleeper only requires a span of 1.2 meter with the load in the middle, the situation in transition zones often involves a row of multiple adjacent hanging sleepers, this can be simulated by the beam model by increasing the span lengths.

The graphs in figure 4.8 visualize the solutions for the beam model for span lengths for 1 to 14 hanging sleepers, that is 1.2 to 9 meters. The displacement at the location of the point load depends on the position on the span where the load is applied, so for each sleeper on the span, that is at each 0.6 meter, is made a separate calculation with the load applied at that point. The result of each of these calculations is denoted with a cross in the graphs, the numbers on the horizontal axis point out to which sleeper number, counted from the side, the cross refers. The results are plotted for halve of the span, since the other halve of the graph would have exactly the same values in mirrored order. The left graph shows what the vertical displacement would be when a load of 80 kN is applied at that point. Since this displacement increases when the load approaches the middle of the span, the displacements are largest at the points farthest from the side.

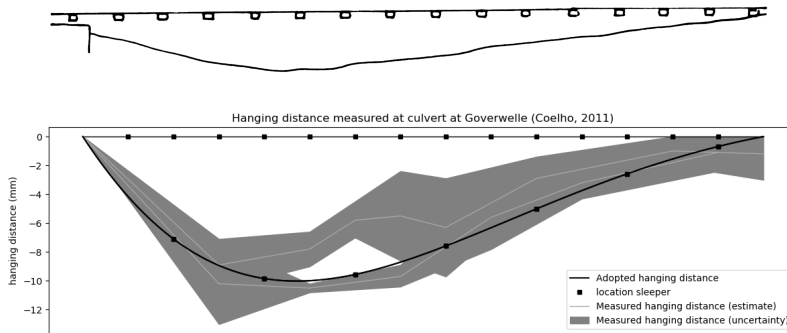


Figure 4.9: Hanging distances of sleepers measured from the culvert (left) at Goverwelle (Coelho, 2011)

If the lines would continue leftwards to the ‘zeroest’ sleeper, the displacement would be 1.4 mm for all lines because this is the displacement of the support when a load of 80 kN is applied there. The right graph shows the spring stiffness that comes with all solutions, that is the force divided by the displacement ( $k=F/u$ ) so this is the inverse of the first graph. Which span length, and thus which equivalent spring stiffness, is used in the calculations will be explained in the next section.

#### 4.1.5. HANGING DISTANCES

The hanging distances of sleepers in a transition zone is derived from the data from the field measurement at location Goverwelle described in 2.5.1 (Coelho, 2011). The estimates of the hanging distance of a number of sleepers on both sides of the culvert are plotted along with their uncertainty margin in figure 4.9. The black line indicates the adopted assumption for the course of the hanging distances over a length 9 meters with 14 hanging sleepers. In order to compare the behaviour of sleepers at different locations, 7 separate calculations are run for the sleepers indicated with black squares on the graph. The calculations are distinguished by the varying hanging distances, as showed in the graph, and by the difference in vertical resistance of the rail.

What span lengths are used for the computational model can directly be derived from figure 4.9, that is 7 different locations at a span of 14 hanging sleepers. The adopted stiffnesses are denoted with red crosses in figure 4.8. Linear elastic solid elements were used in the FE model to model these springs because it was difficult with to model actual spring support in the Kratos software. Table 4.1 below lists the properties for all calculated configurations. It shows that the resistance of the rails will decrease towards the middle of the span, whereas the hanging distance increases towards the middle. From a purely static point of view the stresses on the ballast-sleeper interface will decrease whenever the hanging distance increases, because the counteracting force of the rail resistance will increase and the axle load will stay the same. On the other hand, due to dynamics the sleeper will gain a velocity when it moves down, and when the sleeper will hit the ballast with a velocity this will increase the interface stresses. The calculations of the FE model are hoped to give in insight in how these two mechanism interact.

Sleeper	L <sub>1</sub> [m]	L <sub>2</sub> [m]	From side (figure 4.8)	Spring stiffness [kN/mm]	Hanging distance [mm]
1	1.2	7.8	2	12.6	7.1
2	2.4	6.6	4	3.9	9.84
3	3.6	5.4	6	2.3	9.56
4	4.8	4.2	7	2.1	7.58
5	6.0	3.0	5	2.8	5.01
6	7.2	1.8	3	6.3	2.58
7	8.4	0.6	1	31.1	0.69

Table 4.1: Adopted stiffness values for the equivalent spring for the sleeper (for two rails)

#### 4.1.6. INTERFACE

The contact surface of the sleeper and the ballast are connected with 3D prismatic interface elements, these are developed in collaboration with the software engineer within Deltares. In each time step the distance in between the nodes of both contact surfaces will be checked, if the bodies are physically separated from each other there will be no stresses generated via the interface elements. If the distance between the nodes closes, that is when there is physical contact, the interface will adopt a stiffness, this can be looked at as a spring connection between the two nodes. This stiffness ( $E_{\text{loading}}$ ) should be higher than the stiffness of both bodies to make the interface elements give sufficient resistance. Since the bodies will approach each other in successive time steps, the interface stiffness will be activated already before the surfaces actually make contact to make sure they will not shoot through. The stiffness will be activated exponentially when the nodes approach each other according to the term  $\exp(\epsilon \cdot \text{fac}_{\text{decay}})$ , so the decay factor ( $\text{fac}_{\text{decay}}$ ) can be adjusted such that the activation suits the model as good as possible. Furthermore the interface has been given a second stiffness for unloading ( $E_{\text{unloading}}$ ), so the sleeper will not be kept 'stick' to the ballast. This value should physically be equal to zero, after all there will be no tension in case of unloading, though for numerical calculation reasons this value is set to 1.0. Furthermore the interface elements adopt the Mohr-Coulomb theory to enable shear shift among the ballast-sleeper interface. The cohesion and critical angle parameters however are set sufficiently high to make sure the stresses will stay within their failure envelope and thus show elastic behaviour. The parameters of the interface elements are listed in table 4.2.

Though this method looks well in theory, it turned to be very difficult to script in the Kratos software. In many cases, mainly when the interface stiffness was set sufficiently high, the calculations did not converge. Despite numerous discussions and improvements from the software engineer from within Deltares it wasn't managed to make the calculations run properly for the dynamic calculations. The numerical difficulties are probably due the fact that the distance between nodes approaches zero when the stiffness gets activated over the elements in between this nodes. Particularly in dynamic calculations this is very difficult. The nodes can not simply coincide when the surfaces hit, because the surfaces should still be allowed shift laterally along each other. In order to solve this problems the Kratos script should be investigated in more detail, though it might be possible that this method is not as suitable for this calculation as was expected

1.	$E_{\text{loading}}$ (N/m <sup>2</sup> )	1e11
2.	$\nu_{\text{ur}}$	0.3
3.	$c'$ (N/m <sup>2</sup> )	1.0
4.	$\phi_{\text{peak}}$	30.0
5.	$\psi_{\text{peak}}$	0.0
6.	$ \sigma_{t,\text{cut-off}} $ (N/m <sup>2</sup> )	0.0
7.	Yield function	1.0
8.	$\nu_{\text{un}}$	0.0
9.	$E_{\text{unloading}}$ (N/m <sup>2</sup> )	1.0
10.	$\text{faC}_{\text{decay}}$	1e4

Table 4.2: Parameters interface elements

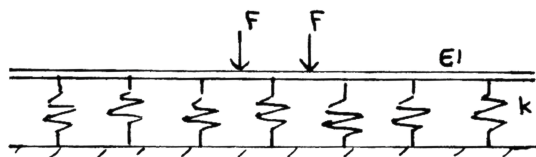


Figure 4.10: Sketch Winkler model

in advance. For this research some parameters were adjusted in such a way that all calculations would run as good as possible, though since there are still questionable things to see in some of the results of the calculations, a certain amount of uncertainty has been taken into consideration.

#### 4.1.7. TRAIN LOAD

When finding the vertical load transferred to one single sleeper by a train axle, one should ideally analyse a dynamic model of a larger part of the railway structure. Since it was not possible to get access to such a model in this research and since it would be too time consuming to build one just for this purpose, the only way to determine the train load was by using a more simplified manner. The railway track was idealized as a continuous beam on a foundation of elastic springs representing the foundation as show in figure 4.10, this is called the Winkler method. The bending stiffness of the rail can be derived using the rail properties, as is explained in 4.1.4. The stiffness of the soil springs, that is the elasticity of the track support, is more difficult to estimate and yet very decisive for the stress distribution over the track. Literature was used (Esveld, 2011) to find a suitable value for this springs.

The model will involve only a vertical train load, for reasons explained in section 2.2. A bogie usually comprises a set of two axles with a distance of 2.5 meters. The second axles will succeed the first one in such a short time it might amplify the resulting stresses, so the Winkler model will employ two axle loads. The maximal axle load on dutch railways is 225 kN, this value matches the axle load of heavy intercity trains in the Netherlands (Coelho, 2011). Since the purpose of this model is to simulate the highest loads expected

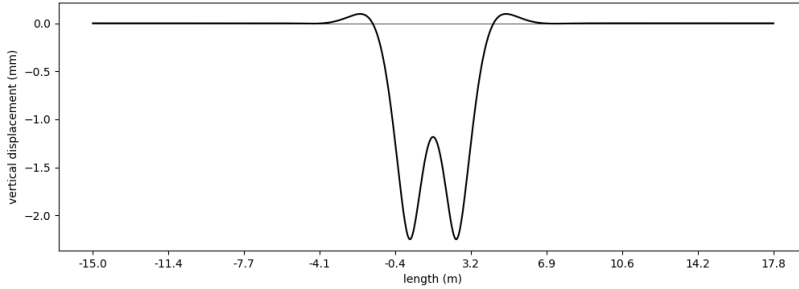


Figure 4.11: Graph static vertical displacement Winkler

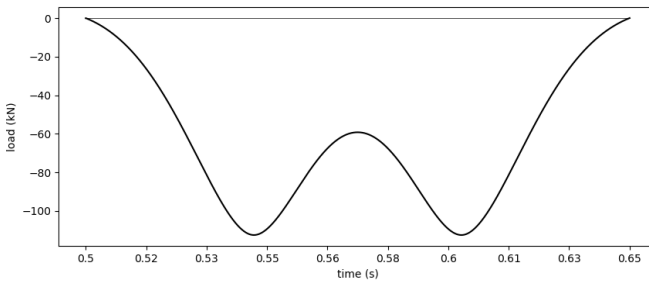


Figure 4.12: Adopted vertical train load on sleeper

on the track, the load of 225 kN is adopted in the Winkler model. The vertical beam displacement over the length can be found by solving the differential equations for the Euler-Bernoulli beam  $\left(\frac{\partial^4 u(x)}{\partial x^4} = \frac{q}{EI}\right)$  for separate sections of the Winkler model using the right boundary conditions. This displacement, plotted in figure 4.11, is the result of a static calculation.

The shape of the rail deformation will be influenced by the velocity because of dynamic effects; the rail will not have enough time to move to a certain position due to its inertia when the velocity will increase, so mainly the right half of the graph will be distorted. The maximal velocity of a dutch train however is in general 140 km/h (excluding high-speed trains and the like), this velocity is assumed to be too low to impose significant influences. This is confirmed by calculations of Varandas (2020), which show a very similar displacement course for a fully dynamic calculation. It is for that reason that there is hold on to this static calculation to determine the load. The load is proportional to the displacement ( $F = ku$ ) so the corresponding force can be found directly from the calculated displacement, this is plotted in 4.12. The scale of the time domain is based on a train velocity of 140 km/h.

Literature is used for validation (Varandas et al., 2017; Paixão et al., 2018; Varandas, 2020; Jain, A., private communications). Furthermore the American Railway Engineering and

Maintenance-of-Way Association presents estimates of the percentage of the axle load carried by one individual sleeper (AREMA Manual for Railway Engineering, Chapter 30, article 1.3.3) and stated maximal 50% of the axle load is carried by one sleeper. This factor seems to be adopted in all literature and is confirmed by the calculation in this chapter as well, so an axle load of 225 kN transfers up to 112.5 kN to one sleeper.

#### 4.1.8. CALCULATION DETAILS

A damping stiffness was attributed with a Rayleigh stiffness value of 0.01 in the dynamic calculation. This value was picked, arbitrary to some extent, by observing what led to a calculation that gave physically the most realistic results. The calculation is carried out in time steps of 0.003 seconds, that is 44 steps (if no extra cycles are required). Since the calculation often gave problems converging, mainly when the interface stiffness was set to high, it was important to pay attention to selecting the right time integration method. The Newmark method was used in this calculation with beta set to 0.25 and gamma set to 0.5 (middle point rule), this is expected to give a stable calculation. In collaboration with the Kratos software engineer from within Deltares is tried to select the right calculation method by selecting the line search strategy and the residual criterion converge criterion. Despite this effort the calculations often got stuck, which seems to suggest that the problem is in the interface method itself. This might have to do with the fact that the method is based on very large stiffness on small distances, which is difficult to realize in dynamic FE calculations.

## 4.2. RESULTS CALCULATION

### 4.2.1. COMPARING HANGING SLEEPERS

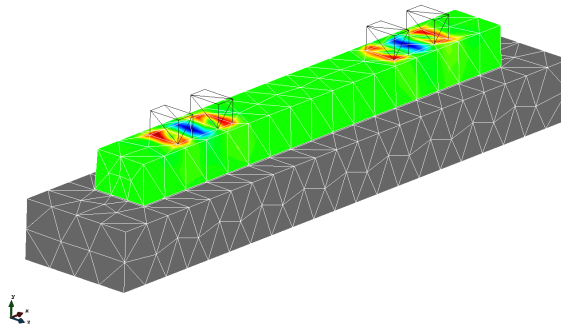


Figure 4.13: Kratos FE model mesh size 0.15

In order to efficiently use the calculation time, it was started to run calculations using a mesh with an element size of 0.15 meters. This led to somewhat rough calculations but good enough for a first analysis and the calculation could be ran within 2 hours which made it workable to use for comparisons. For each of the 7 configurations was investigated what the average stresses at the ballast-sleeper interface were at the moment the maximal train load was applied. The stresses at the ballast-sleeper interface are on

the one hand expected to increase when the hanging distance increases in a dynamic calculations, because a downward velocity will accumulate when crossing the hanging gap and this will lead to a higher force when the sleeper eventually hits the ballast. On the other hand the vertical resistance force of the rail will increase as the sleeper lowers, causing an opposite effect. The first sleeper is a good example for this (figure 4.14), because the rail gives so much resistance at this location that the sleeper barely hits the ballast, so despite the large gap the ballast stresses are very low.

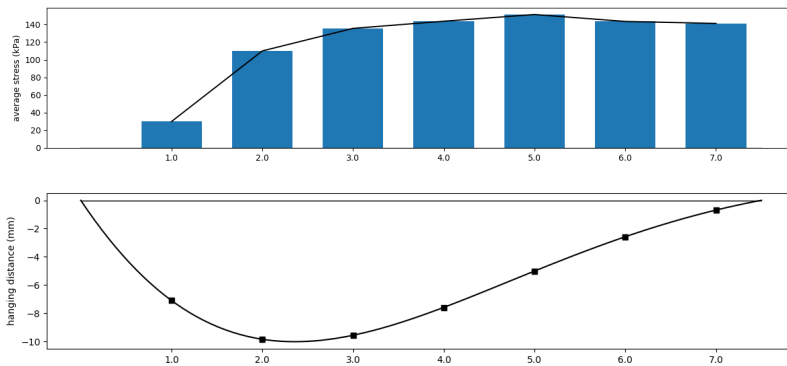


Figure 4.14: Average stresses at the ballast-sleeper interface for different configurations FE-model

A static calculation for the stress on the sleeper soffit can manually be performed; the resultant downward force is the axle load ( $F$ ) minus the spring stiffness for the rail resistance ( $k$ ) multiplied by the downward displacement of the sleeper ( $u$ ), so that is  $F - ku$ . Dividing this resultant downward force by the area of the sleeper soffit gives the average static stress on the sleeper soffit. This is listed in the last column of table 4.3. The numbers give an interesting view on the forces working against each other in this dynamic calculation, concluding that the largest forces will be reached at sleeper number 5. This sleeper will therefore be studied more profoundly in the next section. The bottom row makes a comparison with the stresses on a sleeper without hanging distance, from now referred to as supported sleeper.

Sleeper	Spring stiffness [kN/mm]	Hanging dist. [mm]	Av. model stress [kPa]	Static stress [kPa]
1	12.564	7.10	30.00	31.06
2	3.883	9.84	110.01	99.06
3	2.322	9.56	135.57	120.4
4	2.115	7.58	143.66	128.6
5	2.825	5.01	151.28	131.13
6	6.260	2.58	143.42	128.47
7	31.097	0.69	141.16	120.47
		0.0		150.0

Table 4.3: Stresses ballast-sleeper contact from computational model (dynamic) and from simple static calculation

#### 4.2.2. REFINED CALCULATION

To analyze the behaviour of the sleeper more profoundly is made use of a more refined mesh, using elements of 0.05 m, on the hanging sleeper referred to as sleeper 5 in the previous section. Since the outcomes of the rough calculations from the previous section show that the magnitude of the stress on the hanging sleepers are close to the magnitude of the stresses without hanging distance, a refined calculation is made from the supported sleeper as well. The results of these calculations are shown in this section.

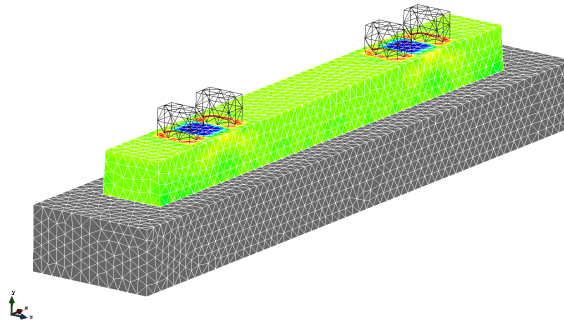


Figure 4.15: Kratos FE model mesh size 0.05

The vertical displacement of both the supported sleeper and the hanging sleeper subjected to the train load (figure 4.16) are plotted in figure 4.17 and 4.18, both measured from one bottom corner of the sleeper. It can be seen that the sleeper somewhat penetrates the ballast at some points, this is acceptable because this way the interface stiffness will be fully activated. Attributing a higher stiffness to the interface elements would suppress the penetration, though this was not possible because it gave problems in the numerical calculation. As expected the supported sleeper is in full contact with the ballast during the loading, whereas the hanging sleeper will only hit the ballast during high loading and will then mostly be stopped in its motion.

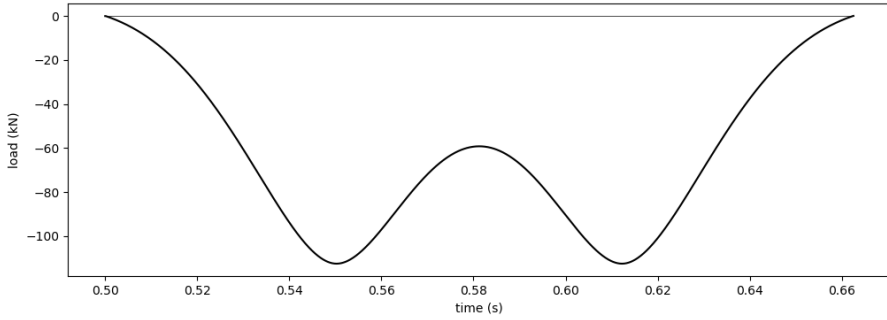


Figure 4.16: Vertical train load applied on sleeper (section 4.1.7)

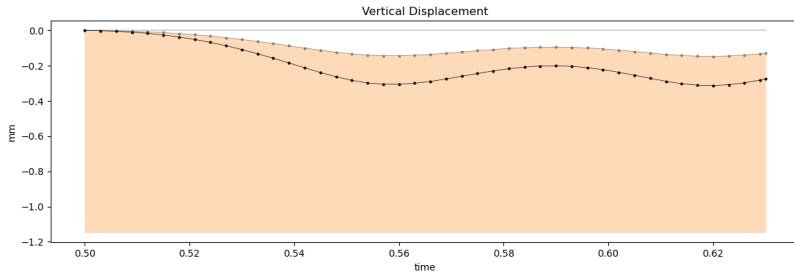


Figure 4.17: Vertical displacement of sleeper (black) and ballast (grey) from calculation supported sleeper

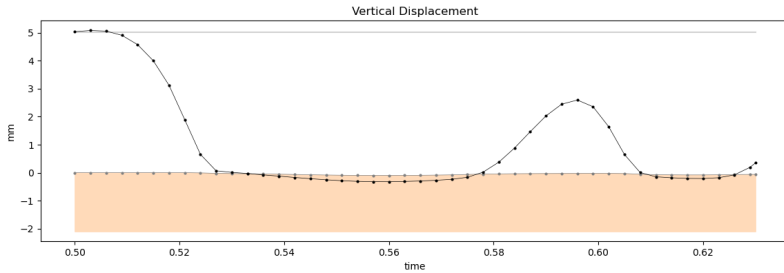


Figure 4.18: Vertical displacement of sleeper (black) and ballast (grey) from calculation sleeper 5

### INTERFACE STRESSES

The most important information that is wanted from this model is the magnitude of the vertical stresses at the ballast-sleeper interface. Figures 4.19 and 4.20 show how the average vertical stress on the ballast-sleeper interface develops over time for the supported sleeper and the hanging sleeper respectively. The grey area covers the range of the deviations, this deviation is partly due to the deformation of the sleeper, but the main cause is

the oscillations in the stresses caused by the interface elements. The stress development of the supported sleeper plotted in figure 4.19 seems to suit well with the applied force. There is always a compressional stress since there is full contact with the ballast and the fact that the load of the second axle ( $t=0.62$ ) barely leads to larger forces than the first axle suggests that the influence of dynamic effects is very small. The displacement of the hanging sleeper in figure 4.20 however does not suit with physics. There are no stresses up until the sleeper hits the ballast at  $t=0.52$ , after which the stresses increase as the load increases, so far it goes well. After this the axle load decreases and in can be seen from figure 4.18 that the sleeper loses contact with the ballast for a while, it is physically not correct that there are still considerable interface stresses present at this moment as the graph implies. It seems like the interface elements are not able to get rid of their stresses as they should in case of unloading. The dotted line indicates what is expected because of the unloading of the sleeper. It seems that the remaining stresses influence the magnitude of the stresses at the second axle load because it adds up the stresses from the second axle load to the residual stresses, it could therefore also be concluded that the results after  $t=0.56$  are worthless.

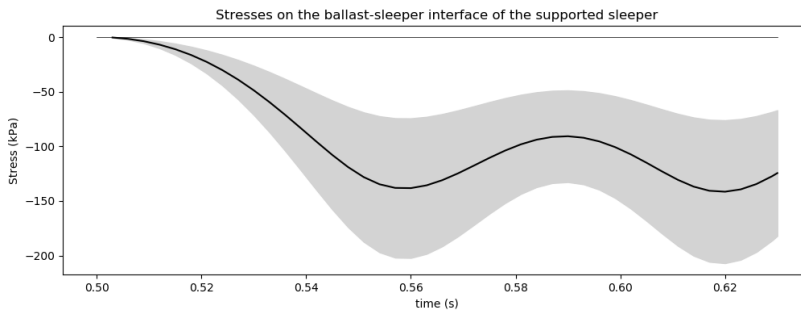


Figure 4.19: Vertical ballast-sleeper interface stresses on supported sleeper over time

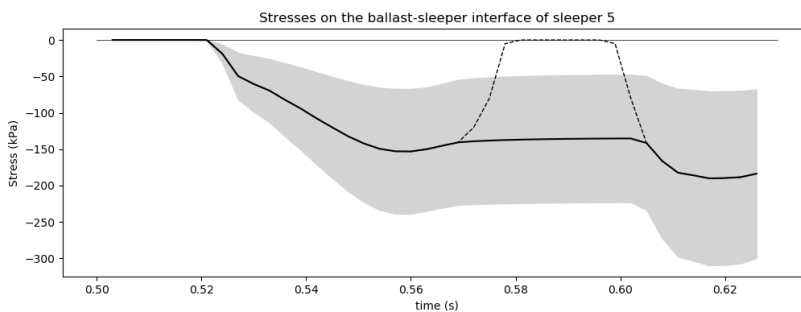


Figure 4.20: Vertical ballast-sleeper interface stresses on hanging sleeper over time

Figures 4.21 and 4.22 show the stresses over the length of the sleeper at the moment the stresses were the highest, that is for both calculations at  $t=0.62$ . The oscillation in

the stress distribution is very troublesome, especially in the case of the hanging sleeper. This has to do with the way the interface elements are programmed in the software, it might have to do with the fact that only part of the elements on the surface are activated and the stresses are therefore focused on these points. It would thus be better to find a way to activate the elements simultaneously on the whole of the surface, so the stresses would be spread out more smoothly. This is however known to be difficult to implement in finite element methods. Anyway the stresses should on average be correct, so by using interpolation it would be possible to get a clear picture of the magnitude of the stresses over the length.

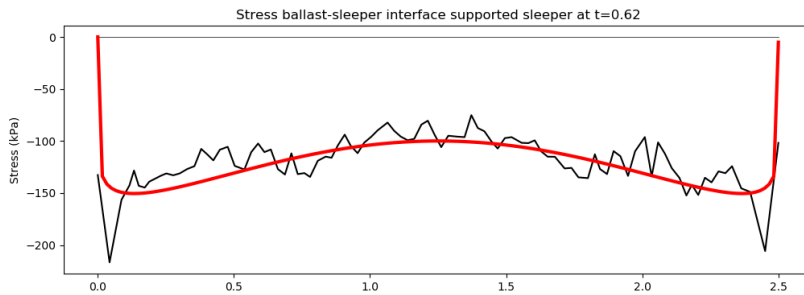


Figure 4.21: Vertical ballast-sleeper interface stresses on supported sleeper at  $t=0.62$

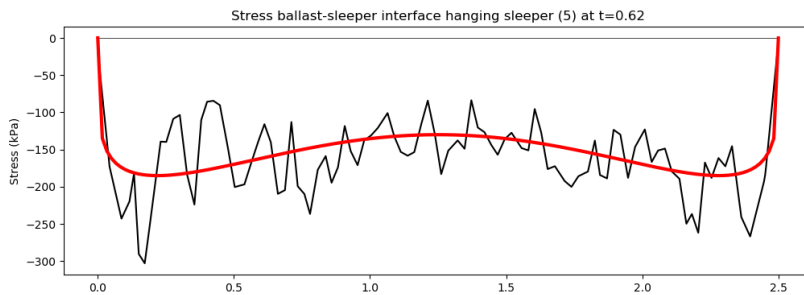


Figure 4.22: Vertical ballast-sleeper interface stresses on hanging sleeper at  $t=0.62$

The interface stresses are higher for the hanging sleeper, close to 200 kPa at the outer ends of the sleeper, though the large oscillations make this value uncertain. The fact that the stresses are highest at the outer ends can be explained by the bending shape the sleeper will adopt; the sleeper will be pushed down at the location of the rails, the middle part will lag behind because of the ballast resistance or because of inertia and thus the outer ends will be pushed down because of this curvature.

### BENDING MOMENT

The vertical deformation of the sleeper is captured in seven time steps ( $t=0.503, 521, 539, 560, 581, 599, 620$ ), this is plotted in figure 4.23 and 4.24. Some lines in the graph, in particular lines later in the calculation when the deformation is largest, show an unsteady course unlike the real situation. This is due to interface problems similar to the problems with the interface stresses as described earlier.

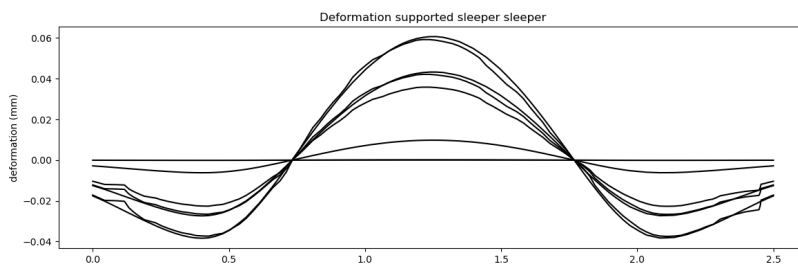


Figure 4.23: Relative deformation over the length of the supported sleeper in 7 equidistant time steps (total displacement per step not included)

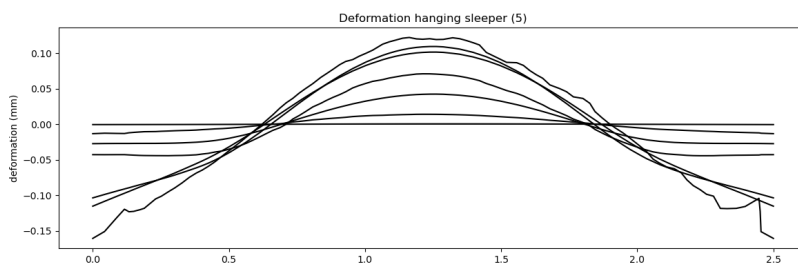


Figure 4.24: Relative deformation over the length of the hanging sleeper in 7 equidistant time steps (total displacement per step not included)

The deformation of the supported sleeper and the hanging sleeper clearly show a different shape. The hanging sleeper (4.24) shows an inverted U-shape, whereas the supported sleeper (4.23) shows the outer ends of the sleeper to be strongly uplifted. This can physically be explained by the fact that the sleeper is pushed down at the location of the rails and because the large mass of the middle part will somewhat resist the displacement, so the outer parts will be pushed downward due to the curvature. In the case of the supported sleeper these outer parts will be pushed upwards by the ballast from the beginning, because there is always ballast-sleeper contact, but for the hanging sleeper this will happen only when it touches the ballast which is not all the time, hence the smaller curvature at the outer ends. Additionally, a dynamic explanation for the shape of the hanging sleeper would be that it equals the shape of the first mode of a free beam.

The bending moments can theoretically be derived by differentiating the displacement over the length  $\left(M = -EI \frac{\partial^2 u(x)}{\partial x^2}\right)$ , however the protuberances in the displacement are strongly amplified by the differentiation. Using some smoothing of the lines, this led to the moment distributions plotted in figure 4.25 and 4.26. The distribution of the moment is a tad different for the supported sleeper and the hanging sleeper, as was expected from the different deformations. The maximal magnitude of the moment seems to be somewhat higher for the hanging sleeper, which is not surprising since the stresses for this sleeper are a bit higher as well.

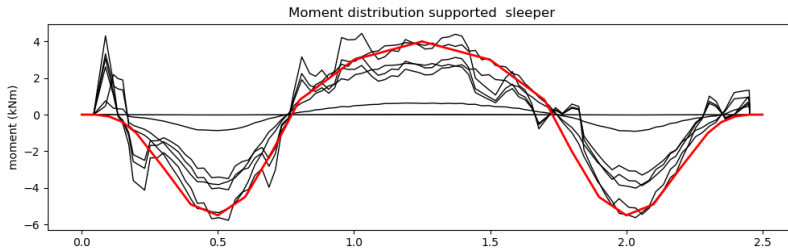


Figure 4.25: Bending moment over the length of the supported sleeper in 7 equidistant time steps

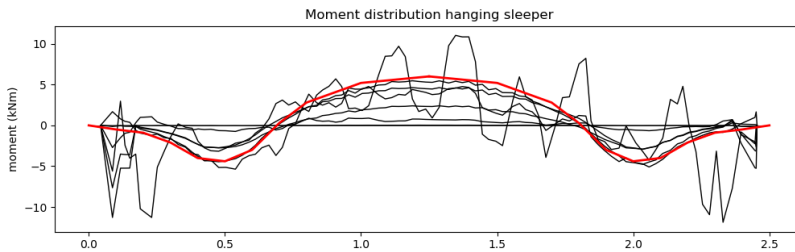


Figure 4.26: Bending moment over the length of the hanging sleeper in 7 equidistant time steps

### ACCELERATION

The acceleration of the sleeper over time is derived from the displacement values from the model calculations. First the velocity is derived ( $v_i = (u_{i+1} - u_i)/(t_{i+1} - t_i)$ ) and from that the acceleration is found ( $a_i = (v_{i+1} - v_i)/(t_{i+1} - t_i)$ ). The results are plotted for the supported sleeper and the hanging sleeper in figure 4.27 and 4.28. Each graph shows the acceleration at two points on the sleeper, namely the points with the largest vertical spacing due to the deformation of the sleeper. The difference in acceleration of the two points on the supported sleeper seems to be substantial, but note that the acceleration is very small here; the sleeper will not move so much since it is from the start resisted by the ballast. The hanging sleeper shows a much higher acceleration, up to  $140 \text{ m/s}^2$ . In the end of the graph there seems to be a significant gap between the acceleration at both points, but note that the lines look very rough at this point which indicates some numerical uncertainties.

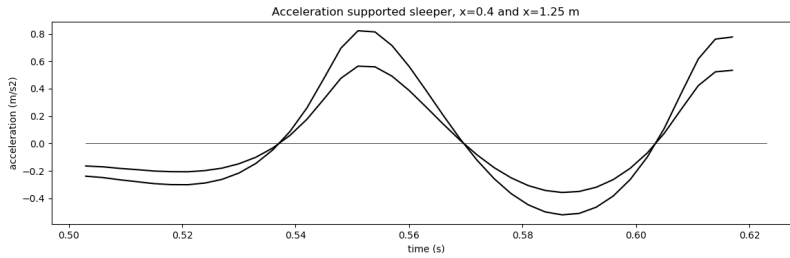


Figure 4.27: Acceleration supported sleeper (midway and 0.4 m from the outer end)

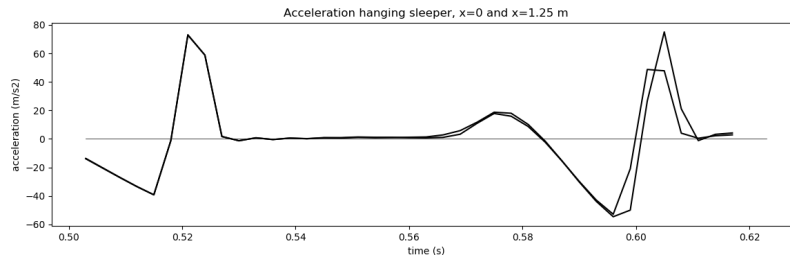


Figure 4.28: Acceleration hanging sleeper (midway and at the outer end)

### 4.3. CONCLUSION

When determining the stiffness values for the linear elastic springs representing the rail resistance, it was found that the influence of the rail was enormous because of the high bending stiffness of the rails. Looking at one single hanging sleeper, the rail stiffness will hardly allow for any vertical displacement, but when looking at multiple hanging sleepers in a row the rail resistance drops increasingly. In this model, the rail resistance was based on a force applied to one hanging sleeper that is part of a row of fourteen consecutive hanging sleepers. In reality, the surrounding beams will each have a large influence on the curvature depending on their hanging distance, their position in relation to the axle load and their dynamic effects. Hence, although this is the best way to express the situation in a linear model of using only one individual beam, the large influence of surrounding sleepers require a larger part of the railway to be modelled to get a good picture of the behaviour of the sleeper.

As expected, the hanging distance on the one hand causes smaller forces on the sleeper because the rail increasingly resists the displacement, but on the other hand, the growing velocity increases the forces on the sleeper. The calculations however showed that the influence of velocity is relatively small and the forces are mainly determined by the rail resistance. This may be caused by the way the interface elements are activated; the stiffness of the interface increases exponentially as the sleeper approaches the ballast, so this might not simulate the smack of the surfaces well.

The calculations show the hanging sleeper takes on larger stresses than a sleeper which is fully supported by the ballast, with normal stresses of respectively 180 and 150 kPa at the ballast-sleeper interface, that is an increase of 20% for hanging sleepers. The stresses are highest at the ends of the sleeper, this is caused by the fact that the outer ends are pushed down due to the curvature of the sleeper.



# 5

## MEASURING INSTRUMENTS

This chapter gives an overview of suitable measuring equipment for the design of the measurement sleeper. Each section will describe a separate instrument type and will make use of precedent experiences to study the applicability of each method to the design of the measurement sleeper. It should be made clear that the emphasis of this research is on the stress measurement on the ballast-sleeper interface, because there is relatively little experience in this type of measurements. Measurements of acceleration and strain are performed more often and therefore the requisite equipment for these measurements is treated more briefly.

### 5.1. MATRIX BASED TACTILE SURFACE SENSORS

#### 5.1.1. BACKGROUND

Pressure sensors are used in a wide range of fields including dentistry, automotive and healthcare applications (Tekscan, 2021). Paikowsky was the first to investigate the application of tactile pressure sensors for geotechnical purposes (Paikowsky and Hajuk, 1997). He concluded that the tactile pressure sensor system provides dynamic normal stress measurements in granular soils to a good degree of accuracy. A small amount of measurements were performed in the following decades using the pressure sensors in railway structures, these will be discussed later on in this section. Tactile pressure sensors are commercially available from various manufacturers, e.g. Pressure Profile Systems, Inc., Sensor Products, Inc., Tekscan, Inc., and Peratech, Ltd. This study focused on the pressure sensors manufactured by TekScan, Inc. because of its wide range of sensor types and because of its precedent uses in similar projects (Stith, 2005; Palmer et al., 2009; Rapp et al., 2012; McHenry, 2013).

#### 5.1.2. SYSTEM COMPONENTS

The matrix based tactile surface sensor (MBTSS) manufactured by Tekscan consists of two thin polyester sheets with lines of electrodes printed on it. The sheets are overlaid such that the lines form rows and columns in a matrix, figure 5.1 give a schematic repre-

sensation of this. The intersection of each row and column is called a sensel. An electrical current will flow through the rows and columns of the matrix, and since the resistance in the circuit of a sensel will change when a pressure is applied or released on the surface, the magnitude of the pressure can be measured at each sensel by measuring the current flow. The output of every sensel on the sensor is given for each time step with an 8-bit system. The sensor is connected to a Tekscan handle which provides current, controls the scanning frequency and sensor sensitivity, converts the analog signals to digital signals and transfers it to a computer. The I-scan software from Tekscan allows for data analysis, e.g. by giving a visualization of the stress development on the surface over time with a 3D video.

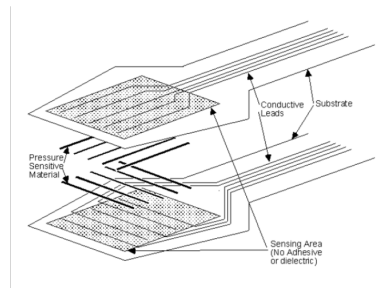


Figure 5.1: Schematic of a tactile stress sensor (from Tekscan)

### 5.1.3. BALLAST-SLEEPER INTERFACE APPLICATIONS

An extensive research on the applicability of tactile stress sensors on a ballast-sleeper interface was described in a thesis report by McHenry for the University of Kentucky (McHenry, 2013). He performed laboratory tests using a concrete, a wooden and a composite sleeper section with a length of 61 cm (24 inch) on a volume of ballast. MBTSS where used to measure the stresses on the ballast-sleeper interface during various loadings on the sleeper sections. McHenry investigated what protection was required for the sensor not to be damaged, as will be elucidated in section 5.1.4. After the MBTSS system was proved feasible in the laboratory tests, field tests where performed on a testing loop. Both the laboratory and the field-test used five different ballast materials (sand, pea gravel, fouled ballast, moderate ballast and new ballast) to study the effects of ballast gradation on pressure distribution. McHenry encountered problems with the calibration of the sensor as will be explained in section 5.1.5. He was not able to find a reliable calibration method, so although the measurement gave useful information on the relative stress data, comparison with other test data was required to obtain absolute values of the data. Stresses up to 1034 kPa (150 psi) were measured with the sensors for axles loads of 353 kN (79415 lbs). The trains speeds in the field measurements were up to 16.1 km/h (10 mph). The conclusion of the study was that MBTSS allows for a viable spacial and temporal analysis of the stress distribution on the ballast-sleeper interface, though it would require an accurate calibration method.

Similar measurements on the ballast-sleeper interface using MBTSS were performed by Gräbe et al. (2016) to investigate the effect of under sleeper pads. Judging by the mea-

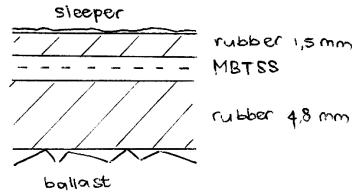


Figure 5.2: Build-up of the protection layers used by from McHenry (2013)

surement data presented in the report this measurement worked very well, though very little information was given about the measurement process. Another application of MBTSS on the ballast-sleeper interface is carried out in the so-called ‘sensor sleeper’ developed by Getzner Werkstoffe GmbH, an Austrian company specialised in manufacturing equipment for railway structures. No technical data was available on the development of this sleeper.

#### 5.1.4. PROTECTION

Given the susceptibility of the sensor being punctured or damaged by the ballast particles, it is important to provide sufficient protection. McHenry (2013) tested four different polyester sheets as a protection layer in a field measurement and concluded each of them provided insufficient protection. Subsequently he performed laboratory tests with rubber protection layers with thicknesses of 0.4 to 3.2 mm and 50A to 70A Shore durometer hardness. Based on this he decided to use a 60A rubber protection layer of 1.6 mm on the concrete side and a 4.8 mm layer on the ballast side (figure 5.2). The thin layer on the concrete-side of the sensor was required to protect the sensor against damages from the raw sleeper surface. He found in the laboratory tests the sensor had to be replaced five times during the experiment because it had reached the end of its serviceable life. The test comprised 80000 load cycles ranging from 9 to 89 kN (2 to 20 kips) with an average of 71.2 kN (16000 lbs), so the average longevity of the sensors was 16000 load cycles. During the in-track testing some sensors were damaged and immediately replaced, though no more information was given about this.

#### 5.1.5. CALIBRATION

The Tekscan sensors require conditioning, equilibration and calibration before use (Palmer et al., 2009). Conditioning involves loading the sensor to a level at or above the anticipated test load several times to reduce drift and hysteresis later on. Equilibration means applying a uniform load to the full active area of the sensor so the software can adopt a scale factor for each sensel such that the digital output of that sensel is equal to the average of all sensels, this way differences in sensitivity between sensels due to manufacturing of repeated use of the sensor are wiped out. The third and most challenging operation in this application is the calibration. During the calibration a certain pressure is applied on the sensor, this stresses should replicate the range of load magnitudes and the stress distribution in the eventual measurement as much as possible. The analog reading from the sensor is converted to digital values, this is called raw data. The value

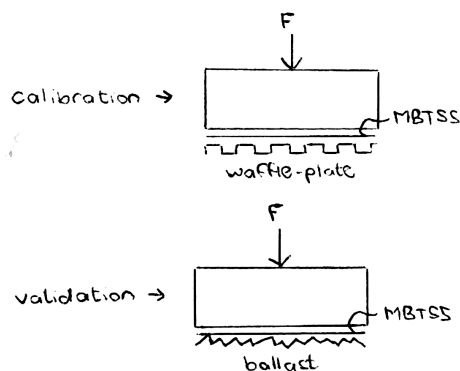


Figure 5.3: Setup of the calibration (top) and validation of the calibration (bottom) used by McHenry (2013)

of this raw data is correlated to engineering units based on the magnitude of the applied pressure. The sensor is typically calibrated using a one-load (also one-point or linear) or two-load (two-point or nonlinear) calibration. As the name suggests, only one load is applied in the one-point calibration and then a calibration line is obtained by connecting the zero point to the calibration point on the sensor output versus load graph. A two-load calibration uses an initial load and a second higher load to generate this line.

The large range of load magnitudes expected and the irregular composition of the ballast particles ask for a distinct calibration method for measuring the ballast-sleeper interface stresses. McHenry (2013) searched for a good way to perform this calibration and decided in collaboration with Tekscan to make use of a machined aluminium waffle plate to apply the load via a surface of 12.8 mm (0.5 inch) separate squares. The waffle plate allows for a consistent control of the contact area but also mimics the compressed contact points to a certain degree. A one-load calibration was conducted using the MBTSS with the aforementioned protection layers, placed on the bottom of a block which was loaded on top, this setup is shown in figure 5.3. After the sensor was calibrated on the waffle plate, the calibration was validated by loading the same block assembly on a ballast bed. It turned out in the validation that the measurement gave completely different loading values on the ballast surface when the same load was used, in other words the calibration failed. It was tried to better replicate the ballast surface by using a waffle plate with smaller squares (6.4 mm) for the calibration, though this barely affected the calibration results. Visualizations of these output are shown in figure 5.4. The report concluded an accurate calibration method for the ballast-sleeper interface is still required to find absolute pressure data, though a conclusive solution for the calibration problem was not given.

#### 5.1.6. RAIL-SLEEPER INTERFACE APPLICATIONS

An extensive study into the applicability of MBTSS for measuring pressures in the rail-sleeper connection was described in the master thesis report of Stith (Stith and Rose, 2004; Stith, 2005). Both laboratory experiments and field measurements were performed

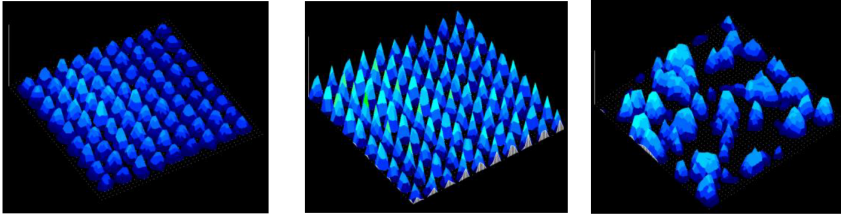


Figure 5.4: Stress distribution shape measured by MBTSS for (left) a 12.8 mm waffle plate, (middle) a 6.4 mm waffle plate and (right) a surface of fouled ballast (from McHenry, 2013)

using the pressure sensors in between the baseplate and the rail of a wooden sleeper. The report gives an extensive step-by-step description of the best way to perform the calibration and the field measurement. Special attention was given to the surface of the baseplate; it was recommended to use a machined baseplate to make sure that the forces are distributed in such a way that they are properly measured by the sensor. The report concludes the technology to be very precise and accurate to determine the rail-sleeper contact stresses when a careful calibration and refinement of the contact surface has taken place.

Another application of MBTSS on the rail-sleeper interface is performed in a study on the rail seat deterioration of concrete sleepers (Rapp et al., 2012). The sensors were, provided with protective polyester layers, placed between the baseplate and the concrete sleeper top in laboratory measurements. Part of the study was to study the influence of the rail pad stiffness by comparing measurement with a medium density polyethylene rail pad and a low modulus thermoplastic vulcanizate rail pad. The use of MBTSS is described as a feasible, non-intrusive means to instrument concrete sleepers to measure rail seat pressure distributions.

## 5.2. PRESSURE CELLS

### 5.2.1. SYSTEM COMPONENTS

Throughout history, various ideas have been put forward to make use of pressure capsules to measure stresses in a railway structure (Watts, 2018). Manufacturer Geokon developed pressure cells using this method in a way it is suitable for granular stress measurements. The pressure cell comprises two cylindrical disks with a diameter of 230 mm which are sealed at their periphery and filled with de-aired hydraulic fluid. When a pressure is applied to the cell, the change in fluid pressure is measured in the transducer and converted to an electrical signal that can be translated by the computer. This way the pressure cell offers a reliable value of the average load magnitude on the surface of the cell. Though regular pressure cells will be damaged because of the high stresses transferred by the ballast particles, the Geokon 3515 type (figure 5.5) is much thicker and is sufficiently able to resist the high stresses at the ballast-sleeper interface.

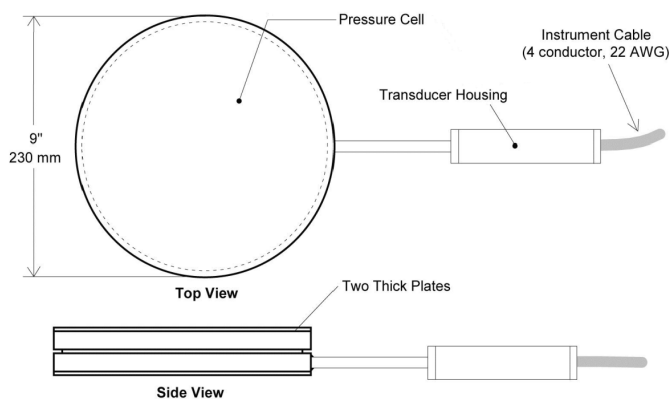


Figure 5.5: Geokon 3515 (from Geokon)

### 5.2.2. PREVIOUS APPLICATIONS

After the study of McHenry showed problems with calibration and protection, a search for a more durable and reliable measurement system for the ballast-sleeper interface arose. In that spirit Rose et al. (2017) investigated the applicability of pressure cells on both concrete and wooden sleepers. Existing tracks were lifted in order to fix the cells underneath a row of sleepers at the location of the rail. Observations showed that due to looseness of the ballast after installation, a gap formed between sleeper and the cell, so that little to no force was transferred to the cell. It was tried to solve this by shimming the cells to bring them flush against the sleeper, but extremely high forces were measured as a result. All in all it seemed it was not managed to measure the stresses in a correct, non-invasive way.

Successful measurements of the interface stresses on wooden sleepers were performed by Watts (2018). Because of the fixation problems from Rose et al. the pressure cells were recessed in the bottom of the sleeper; a recess was milled in the sleeper soffit, the pressure cell was placed in this hole and shut down with a textured surface plate. Due to the size and the shape of the pressure cell no more than two cells were said to fit in one sleeper.

## 5.3. ACCELERATION MEASUREMENTS

### 5.3.1. PIEZOELECTRICITY

A great number of sensing principles can be used to measure acceleration (e.g. capacitance, piezoelectricity, laser based, magnetic induction, optical, electromechanical servo-hydraulics, resonance) though the vast majority of conventional accelerometers is based on piezoelectric crystals (Ngamkhanong et al., 2018). The acceleration of a mass generates a proportional stress which accumulates a measurable piezoelectricity. This is a relatively simple method to measure the acceleration in one direction. A drawback of the piezoelectric crystals is that they are often considered too big and clumsy (Andrejašič,

2008).

### 5.3.2. MEMS

In order to overcome the aforementioned drawback, a new type of sensor named the micro electromechanical system (MEMS) was developed (Ngamkhanong et al., 2018). MEMS measures the capacitance changes due to distance between capacitor plates, and uses this to convert it to the acceleration. If one includes sets of capacitors turned in perpendicular directions, one can measure acceleration in two or three axes (triaxial). An advantage of this type of sensor is its small dimensions. Moreover, MEMS sensors are able to resist extreme temperature, vibrations or shock conditions (Ngamkhanong et al., 2018) and are available in wireless systems which is more convenient for in-field measurements. Since this type processes much more data than the traditional accelerometer, more sophisticated equipment is required for post-processing.

### 5.3.3. RAILWAY MEASUREMENTS

In the field measurement at location Goverwelle accelerometers were used on the sleepers (Coelho, 2011) as well as on the approach slab (Hölscher and Meijers, 2009) and in the soil (Coelho et al., 2010). Both uniaxial and triaxial accelerometers were used in the project, though it could not be found from literature which types of sensors were used. Rose et al. (2015) used accelerometers on concrete sleepers and described this as inexpensive, quickly installed, non-invasive, durable and reusable measurement tools. It is not described which type was used, though judging by the size and the weight of the accelerometers, that is respectively only 13 mm long and less than 3 grams, presumably MEMS accelerometers were used here. Paixão et al. (2018) used both piezoelectric and MEMS accelerometers on concrete sleepers, though gave no further explanation about this either. Due to the fact that there was little attention paid to these acceleration measurements and clear measurement results were presented, it is assumed that the acceleration measurement has not led to any problems.

## 5.4. STRAIN MEASUREMENTS

### 5.4.1. STRAIN GAUGES

The most common sensor for measuring the response of in a structure is the strain gauge. A typical strain gauge comprises a long conductive strip in a zigzag pattern of parallel lines (figure 5.6). If this conductor is stretched within the limits of its elasticity, it will become narrower and longer, which increases its electrical resistance end-to-end. From the measured electrical resistance, the strain and thus also the induced stress can be derived.

### 5.4.2. FIBER BRAGG GRATING

Nowadays optical fibre sensors are often used as an alternative for strain gauges for structural sensing (Ngamkhanong et al., 2018). Fibre Bragg Grating (FBG) is an intrinsic sensor, this means it uses the optical fiber as the sensing element. Each FBG consists of periodic index changes in the core of the fibre. When a spectrum of light propagates through this grating a specific wavelength, the so called Bragg wavelength, is reflected

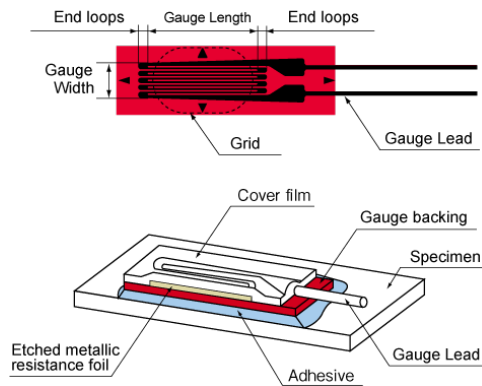


Figure 5.6: Strain gauge configuration (from [https://tml.jp/e/knowledge/strain\\_gauge/about](https://tml.jp/e/knowledge/strain_gauge/about))

back, while the rest of the spectrum is transmitted unaffected. When an external strain is induced, the change in distances will result in a shift in the reflected wavelength, this is shown in figure 5.7. By capturing the reflected light, strain values can be measured dynamically. An advantage of the FBG technology is that measurement points can be fabricated as an array of independent sensors along the same fiber, enabling strain measurements at multiple points along a line.

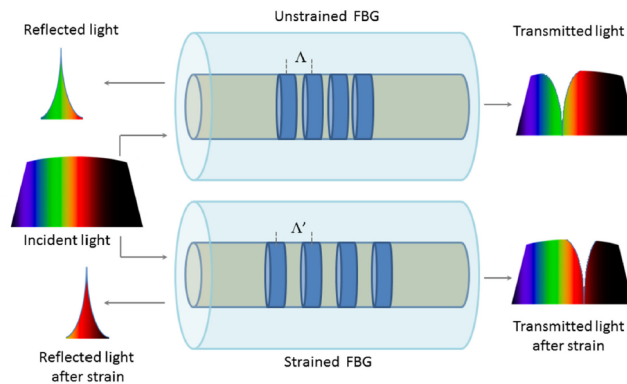


Figure 5.7: Schematic of the working principle of FBG sensors and its response to strain (from Massaroni et al., 2015)

### 5.4.3. SLEEPER BENDING MEASUREMENTS

An extensive study on strain gauges was performed by Edwards et al. (2017) to determine the bending moment in concrete railway sleepers. He used gauges with a relatively long length (30 mm) to be able to span multiple pieces of aggregate and sections of mortar paste within the concrete element. He equipped ten sleepers with each five gauges longitudinally fixed at the side near the top surface of the sleeper. Attention was paid to an adequate protection for the strain gauges, comprising rubber layers and tape. He

concluded the instrumentation methodology and deployment to be successful in measuring bending strains. A similar measurement was conducted by Tran et al. (2020) with seven strain gauges at the side of a sleeper and an eighth gauge on the opposite face in the middle of the sleeper. This measurement was successfully used as a validation.

A so called 'smart sleeper' was developed (Tran et al., 2020) which makes use of 6 FBR sensors embedded in the core of the concrete sleeper. The sensors are situated at the two rail seats and in the middle of the sleeper. This design is used at several sites in Europa (Consolis, private communication) and is said to give reliable data on the longitudinal strain of the sleeper.

#### 5.4.4. AXLE LOAD MEASUREMENTS

Coelho (2011) described how in the field measurement at location Goverwelle strain gauges were used to measure the axle load on the rails. The strain gauges were placed on the rail web, at the neutral axis level, measuring the strain in vertical direction. In this way the bending of the rail has no influence, thus the load could be derived from the shear force only. Two strain gauges were glued on each side of the rail web to account for eccentricity effects, and dummy sensors were added for compensation of temperature effects. This method was found to be a reliable way to measure the vertical load on the rails.

Gao et al. (2017) attached strain gauges to the prestressing wires right below the rail seats before the concrete was poured inside the form, such that the strain gauges would be embedded into the concrete in a vertical orientation. This way the vertical compressive strains could be captured while the axle loads were applied in a laboratory test.

## 5.5. CONCLUSION

The two suitable options for measuring the normal stresses at the ballast-sleeper interface are the pressure cells and the MBTSS. Pressure cells comprise two stiff plates with hydraulic fluid in between, by measuring changes in fluid pressure the total pressure on the plate can be measured. A previous application of the pressure cells in a ballast-sleeper measurement showed the attachment of the instrument to the sleeper leads to problems in the measurement. Also the pressure cell gives no information about the distribution of the stresses. The MBTSS comprises a matrix of electrically conductive lines and uses its change of conductivity when a pressure is applied on the surface to measure the magnitude of this stresses. This instrument is very suitable for a detailed measurement of the force distribution over a surface at high measuring frequencies. A previous ballast-sleeper interface measurement with MBTSS showed the instrument to give reliable results, though the calibration of the sensor is a major challenge in this type of measurement.

Acceleration can be measured by accelerometers, the most common types are the traditional piezoelectric accelerometer or the more sophisticated MEMS. By means of integration, this measurement can also provide information about speed and displacement.

Strain measurements are generally often performed with strain gauges. An emerging alternative for the strain gauges is the fiber method Fiber Bragg Grating, with which multiple strain measurements can be performed on a line. Both acceleration and strain measurements have been used extensively in previous railway analyses, this did not lead to problems and gave clear measurement results.

# 6

## DESIGN SLEEPER

This chapter will describe the best way to design the measurement sleeper to meet the requirements made in chapter 3. The first part of the chapter will describe the basic idea for the measurement of the ballast-sleeper interface stresses, the measurement of the velocity of the sleeper and the additional measurements for validation. In section 6.2 an analytic calculation of the sleeper was added in addition to the computational model in order to substantiate the presented measurements. In the following sections each of the measurements will be explained separately in more detail. The chapter will conclude with an overview of the recommended measurement methods on the sleeper.

### 6.1. BASIC DESIGN IDEA

#### 6.1.1. BALLAST-SLEEPER INTERFACE MEASUREMENT

The main measurement, that is the measurement of the ballast-sleeper interface stresses over time, will be measured by the MBTSS. These sensors will be fixed at the bottom of the sleeper. The arguments for this method and the important details for this measurement are explained in section 6.3. An important problem with the MBTSS in this measurement is the calibration, as was described in the previous chapter. Some advice will be given on the calibration procedure, but laboratory test will eventually have to show whether and to what extent a solution will be found. It is assumed a complete solution will not be found, and thus additional measurements will be necessary to confirm the absolute values of the stresses measured, these validations will be explained in subsections 6.1.3 and 6.1.4.

#### 6.1.2. VELOCITY MEASUREMENT

The best way to measure the vertical velocity of the sleeper is by measuring the acceleration, the velocity can be derived by integrating the acceleration over time. Although the numerical integration inevitably leads to some loss in accuracy, this method is sufficiently reliable because it is a solid, cheap and feasible measurement method with a lot of experience and which can easily accommodate multiple sensors. Details about the

acceleration measurement are described in section 6.5.

### 6.1.3. VALIDATION VERTICAL STRESSES

The first validation will be derived by equating the sum of the vertical forces with the mass times the acceleration of the sleeper, according to Newton's second law ( $\sum F = m\ddot{u}$ ). Firstly the load on top of the sleeper, that is the train load, will have to be measured as well (6.4). Furthermore, the vertical acceleration of the sleeper must be measured (6.5), taking into account that the beam also has a possibility of rotating and deforming. Since the deformation is expected to be very small, the sleeper can be considered as point mass. The acceleration measurement must be organized in such a way that the acceleration of the center of mass can be determined. The data obtained from these measurements makes it possible to also perform an additional validation in case the beam would show rotation, namely by applying Newton's law to the sum of moments ( $\sum M = J\ddot{\theta}$ ). A linear calculation of a sleeper presented in section 6.2 will support this validation.

### 6.1.4. VALIDATION MOMENT DISTRIBUTION

The second validation is to be performed by determining the moment distribution over the length of the sleeper. This information can relatively simple be found and gives a good picture of the stress distribution over the length of the sleeper. The two most obvious methods to find the moment distributions are by using the vertical displacement or by using the longitudinal strain. Vertical displacements can be differentiated over the length to find the moment distribution ( $M = -EI \frac{\partial^2 w}{\partial x^2}$ ). The required displacement data can be obtained via acceleration measurements, which can conveniently be combined with the acceleration measurement described above. The double differentiation over the length however demands displacement data for three points to derive one average value for the moment. Considering that the displacement values are obtained by integrating the acceleration measurements, this method is all in all inaccurate and not so reliable. Measuring longitudinal strain in the sleeper is proved to be a more reliable way of finding the bending moment. In section 6.6 will be explained what is the best way to perform this measurement.

## 6.2. ANALYTICAL CALCULATION

A linear model was used to analyze the significance of the acceleration in the validation of the sum of the vertical stresses and to estimate the influence of an uneven wheel loading. The model comprises a rigid beam with mass  $m$  and moment of inertia  $J$  and two degrees of freedom, i.e. vertical displacement  $u$  and rotation  $\varphi$ , as shown in figure 6.1. The ballast was represented by spring support  $k_b$  (see figure 4.3 for stiffness) and the rail resistance was applied via two springs  $k_r$  just like in the computational model (section 4.1.4). The train load was applied via sinusoidal forces  $F_L$  and  $F_R$ . The solution of this model is elaborated in appendix A.

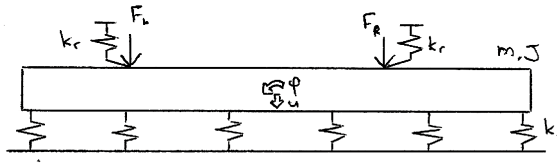


Figure 6.1: Display analytic model

### 6.2.1. SUM VERTICAL STRESSES

Firstly the influence of the inertial force was analyzed by modelling a fully supported sleeper, that is without hanging distance. The value of  $k_r$  is not so important here because the displacement will largely be determined by the ballast stiffness. The right graph in figure 6.2 shows the load on top of the sleeper, i.e. the train load minus the resisting force of the rail, with a green line. The blue line shows the total upward force from the ballast on the sleeper. The inertial force, that is the sum of the forces denoted with the red line, is clearly determined by the eigenfrequency of the model which is much higher than the frequency of the train load. The force has a magnitude of 0 to 8.5 kN, that is no more than 8% of the total force, this corresponds with an acceleration up to  $23.1 \text{ m/s}^2$ . The relatively small contribution of the inertial force shows the acceleration is not so relevant in the summation of vertical forces as the sleeper is fully supported by the ballast.

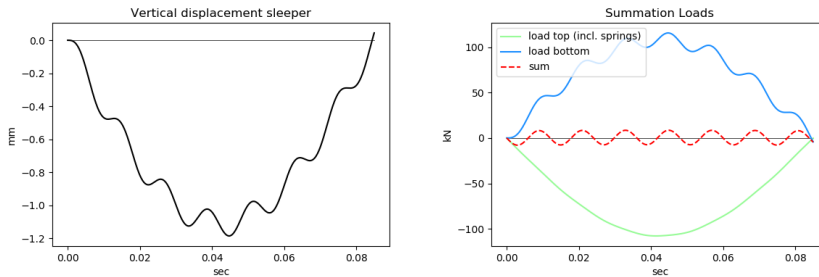


Figure 6.2: Vertical displacement (left) and summation of the vertical loads (right) on a supported sleeper from analytical calculations

### 6.2.2. INFLUENCE HANGING DISTANCES

The acceleration is expected to be relevant in the case of hanging sleepers, this is analyzed with the analytic calculation by setting the ballast stiffness  $k_b$  to zero. The spring stiffness  $k_r$  is very important here since it is the only constrain left, therefore all stiffness values presented in table 4.1 are used for comparison. The red line in the graphs in figure 6.3 denote the spring with the lowest stiffness ( $k_r=2.115 \text{ N/m}$ ). In reality, the sleeper in most of these calculations will be stopped by the ballast at some point in their displacement, depending on the magnitude of the hanging distance. The acceleration is thus not expected to exceed  $100 \text{ m/s}^2$ , this is in line with the results of the computational model. This corresponds with an inertial force of 36.9 kN, which is highly significant in the force summation, although it will decrease very fast when the sleeper touches the ballast. The

analytic model could be extended by inserting a spring when the displacement of the sleeper bridges a certain hanging distance to also find the ballast forces. However, because of the large acceleration it is recommended to involve the acceleration in the sum of the forces on hanging sleepers in order to get a good picture of the stress development.

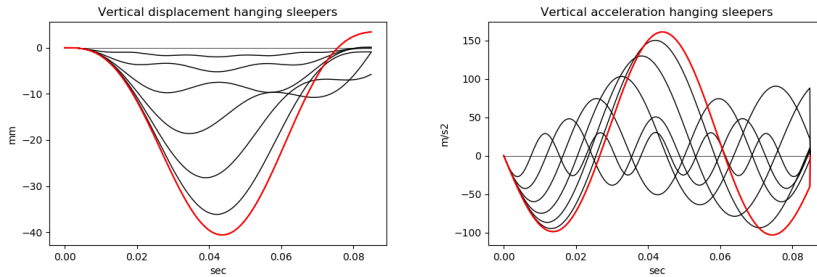


Figure 6.3: Vertical displacement (left) and acceleration (right) of hanging sleeper with varying rail resistances, from analytical calculations

### 6.2.3. ROTATION SLEEPER

In section 2.2 was explained the sleeper might be subjected to an uneven load because of curves in the track. Esveld (2001) stated the proportion of the extra wheel load on the outer rail in curves in connection with non-compensated centrifugal force is usually up to 10 to 25% of the static wheel load. In order to estimate the increase in stresses at the ballast sleeper interface because of this force, only one of the wheel loads in the analytical model was increased by 25%. Figure 6.4 shows the stresses at one end of the sleeper increase with a factor of 1.58. The instruments on the measurement sleeper should be able to take on this increase in stresses as well, in case the sleeper will be placed in a curve. It should be noted here that this factor may be lower in reality because of the bending stiffness of the sleeper and the nonlinearity of the ballast, which is not included in this calculation.

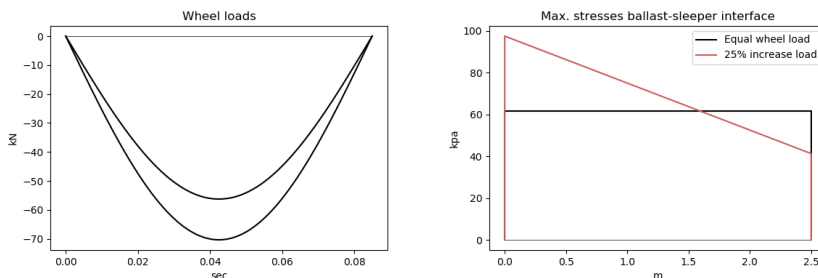


Figure 6.4: Wheel loads (left) and stresses at the ballast-sleeper interface in comparison with centrifugal force (right)

## 6.3. BALLAST-SLEEPER INTERFACE

### 6.3.1. CHOICE MEASUREMENT METHOD

The best instrument for measuring stresses at the ballast-sleeper interface is found to be the MBTSS, described in section 5.1. The possibility of pressure cells is rejected because of the fixation problems of the instruments and because of the impossibility of measuring more than two normal stress values on the sleeper soffit, this is explained in 5.2. An important requirement for the measurement sleeper is to measure the stress distribution over the ballast-sleeper interface as detailed as possible, the pressure cells are not able to meet that requirement.

### 6.3.2. UNDER SLEEPER PAD

In section 5.1.4 was described how the 4.8 mm rubber protection layer offered an average MBTSS longevity of 16000 load cycles in the laboratory tests and had to be replaced several times in the field measurement. This is not sufficient, as the product requirements (chapter 3) specify that the service life of the measuring equipment must be at least one maintenance cycle. It is assumed that the 1.5 mm layer at the concrete-side of the sensor did suffice, since the concrete is relatively harmless compared to the ballast. For the ballast-side protection is sought for a more protective layer.

Better protection was found in the form of an under sleeper pad (USP), for they are designed to provide protection to the sleeper during the whole of its lifetime. Getzner, an Austrian company specialized in all kinds of railway equipment, offers a wide range of USP's with the aim of reducing vibrations and offer protection in order to elongate the service life. The pad comprises an elastic layer with a bedding modulus of 0.10 to 0.32 N/mm<sup>3</sup> with a protection layer on the bottom side of it (Loy, H., private communications). The top of the pad is finished with a connection layer to achieve a good connection with the beam, a choice can be made between a flock connection layer or a mesh connection layer. The choice of which connection layer is most suitable in combination with the MBTSS is left to the executors of the measurement.

### 6.3.3. CALIBRATION

The calibration of the MBTSS proved to be very difficult for ballast measurements, so it is very important to investigate this in laboratory tests prior to the field measurement. The best calibration method found in literature is the method involving machined waffles plates (McHenry, 2013), as described by in 5.1.5, though this method did not lead to a properly working calibration. Since the waffle plate squares apparently do not replicate the ballast particles well enough, a better method might be to calibrate the sensor directly on a ballast bed. It is expected that the core of the problem is in the distribution of the forces of the ballast particles; a lack of spread can cause the force points to disappear between the sensels. It is expected that the USP, being much stiffer than the rubber layer used by McHenry (2013), will solve or at least decrease this problem. Laboratory test are however required to investigate what method works, contact could be made with Tekscan to further discuss how the calibration should be approached. Note

it has been taken into account in the design that a fully successful calibration will not be found and validations are build in to confirm the stress values.

## 6.4. RAIL-SLEEPER INTERFACE

### 6.4.1. CHOICE MEASUREMENT METHOD

Several methods mentioned in the previous chapter could be used to measure the stresses at the rail-sleeper interface. Section 5.4.4 first describes a method to use strain gauges on the rail to measure the shear force in the rail. Though this method proved to give reliable values for the axle load, it doesn't give the actual values of load transferred to the sleeper. The axle load is in practice always distributed over multiple sleepers and in the case of hanging sleepers it might be difficult to predict to what extend. It is thus preferable to measure the vertical rail-sleeper interface stress in a more direct way. Section 5.4.4 also described a method where strain gauges are placed in vertical direction underneath the rail pads, in order to derive the train load from the compressional strain. This method would require to place the equipment already in the manufacturing process of the sleeper, which is not the case for the rest of the design. It is for that reason that it is chosen to use MBTSS at the rail-sleeper interface to measure the contact stresses.

### 6.4.2. FORCE TRANSFER

To measure the stresses transferred to the sleeper at the rail-sleeper connection, the stresses should be measured in between the baseplate and the concrete of the sleeper. Figure 2.4 shows a cross-section of this connection. It should be made sure all vertical stresses are indeed transferred via this interface, after all the baseplates are connected to the sleeper with prestressed bolts at the outer edges of the plate. If the plates are pressed down by the rail, this might lead to a relaxation of the bolts causing a decrease of the stresses on top of the plates by the bolts, so not all vertical stresses will be captured at the interface below. To investigate this, the measurements of Rapp et al. (2012) were used, he performed laboratory tests on the rail-sleeper interface of concrete sleepers using MBTSS. Vertical loads of 145 kN were applied to one of the two rails on a sleeper, comparing two varying baseplate pads. He found for both pads the stress distribution was mainly limited to an area in the middle of the surface and no stresses developed at the outsides, which means the plate bends and all stresses are transferred via the middle of the plate right under the rail. The tension of the bolts is thus not affected and it can safely be assumed that all stresses are captured at the baseplate-concrete interface.

To determine the required stress range of the instrument, the measurement results of Rapp et al. (2012) are studied. He applied a load of 145 kN on one rail, this would be a total load of 290 kN if it was applied on both rails and since only 50% of the axle load will be transferred to one sleeper it corresponds with an axle load of 580 kN. This led to stresses up to 27600 kPa (4000 psi) for a stiff baseplate pad, a less stiff baseplate pad spread the stresses more leading to lower stresses. Assuming a proportional stress distribution for a smaller load, that is 225 kN as expected in this measurement, stresses up to 10700 kPa

are expected. Note the sensor should be placed underneath the baseplate pad and extra layers are required on both sides on the sensor to protect it from shear forces and puncture damage, according to Rapp et al. (2012) this can be achieved with sheets of respectively polyethylene terephthalate (0.18 mm) and polytetrafluoroethylene (0.15 mm).

## 6.5. ACCELERATION

### 6.5.1. MEASUREMENT TYPE

The accelerations has to be measured in one direction, this measurement can be performed with either MEMS or more traditional instruments, as described in section 5.3. It is recommended to use MEMS, because these are smaller and therefor much more convenient to fix on the side of the sleeper in a way they will not be damaged by the ballast particles. The final choice for which type of accelerometer is to be used is left to the execution phase, for it will probably be a more practical and economical consideration. The main requirement is that the instrument meets the prescribed features described in chapter 7 and that it can take a measurement at the designated positions on the sleeper.

## 6.6. STRAIN

### 6.6.1. CHOICE MEASUREMENT METHOD

In the choices for the method of the strain measurement, the calculations of the computational method as described in section 4.2.2 are used, this will be explained in more detail in the next chapter. Since the sleeper is not subjected to a normal force in longitudinal direction, measuring the longitudinal strain at only position at a cross-section is enough to determine the magnitude of the moment. The strain sensors should be positioned as far from the middle vertically as possible because then the stresses are the largest and can thus be measured best. It is not possible to place the sensors on top because the rails are there, so they should be fixed on the side, but as high to the top as possible. Note prestressing stresses are ignored because the concrete is considered in its linear elastic stage. It is thus very important for the strain sensor to be accurately calibrated in such a way that the strain is zero when the sleeper is unloaded. Also the height at which they are mounted must be accurately registered in order to calculate the moment afterwards.

It is recommended to use fibers for the measurement (section 5.4.2) because with this method strain can be measured over the entire length of the beam. This guarantees that all peaks in the moment distribution are measured, also if this peak is at a slightly different location along the length than expected. If, for example for financial or implementation reasons, it is decided to perform strain measurements only on smaller sections, or by using strain gauges, it is important that the strain is measured at the points where the moment peaks are expected, these locations are explained in the next chapter.

## 6.7. ELECTRICAL RESISTANCE

Since all instruments are electrical devices some attention should be paid to the electrical resistance of the sleeper, concerning issues like stray current, EMC and short circuits. Safety- and energy supply departments of the railway management will make sure the equipment will not influence the functioning of the railway, though it should also be made sure the currents of the railway (e.g. traction current or track circuit) will not influence the measurement instruments. This will not be discussed further in this report because it is outside of the scope of the research, though some attention will have to be paid to this topic when carrying out the measurement. It should be mentioned however that these issues are not mentioned in the literature on any of the precedent railway measurements described in this report, so it is not expected to cause any problems.

## 6.8. CONCLUSION

An overview of the recommended measuring equipment is showed in figure 6.5. The MBTSS spread across the underside of the sleeper will measure the ballast-sleeper interface stresses and the accelerometers will provide the vertical velocity of the sleeper.

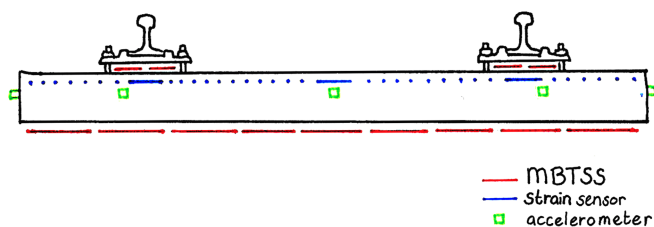


Figure 6.5: Overview of the design of the measurement sleeper

Since the measurement of the MBTSS at the sleeper soffit comes with uncertainties, it is recommended to perform additional measurements in order to capture the moment distribution over the length of the sleeper and the sum of the vertical forces on the sleeper as a validation of the magnitude of the normal stresses at the ballast-sleeper interface. The moment distribution can be found by strain measurements over the length of the sleeper. MBTSS can be used at the rail-sleeper interface in order to measure the vertical load on top of the sleeper. Analytic calculations showed the acceleration should be involved in the summation of vertical forces as well in order to validate the stress magnitude on hanging sleepers. The analytic calculation also showed uneven train loads might increase ballast-sleeper interface stresses up to 58%, so the instruments should be able to measure these stress magnitudes as well.

# 7

## IMPLEMENTING CALCULATIONS

Whereas the previous chapter explained the measurement methodology, this chapter will elaborate on the precise properties of the measurement instruments based on the computational model calculations. The measurement of the stresses at the ballast-sleeper interface, the stresses at the rail-sleeper interface, the acceleration and the strain will each be treated separately. Since the frequency domain is an important property of the measuring instruments in dynamic measurements, these domains are carefully determined for all sensors. Furthermore the range of magnitudes and the required sampling frequency of the values to be measured are derived.

### 7.1. BALLAST-SLEEPER INTERFACE

#### 7.1.1. FREQUENCY DOMAIN

To determine the frequency domain of the normal forces in the ballast-sleeper interface, the results of the calculations with the computational model as described in 4.2.2 were used. The calculated average stress on the supported sleeper and the hanging sleeper are plotted in respectively figure 7.1 and 7.2 with a solid line. These lines are used to derive a Fourier series, these are plotted in dashed lines.

$$s_N(x) = \sum_{n=0}^{30} \left( a_n \cos\left(\frac{2\pi}{P} nx\right) + b_n \sin\left(\frac{2\pi}{P} nx\right) \right) \quad (7.1)$$

$$\begin{aligned} a_n &= \frac{2}{P} \int_P s(x) \cdot \cos\left(\frac{2\pi}{P} nx\right) dx \\ b_n &= \frac{2}{P} \int_P s(x) \cdot \sin\left(\frac{2\pi}{P} nx\right) dx \end{aligned} \quad (7.2)$$

The Fourier series ( $s_N(x)$ ) are defined by the summation in equation 7.1, with  $P$  being equal to the duration of calculated interval, that is in this case 0.12 seconds. The Fourier coefficients  $a_n$  and  $b_n$  are found by using numerical integrations as defined in equation

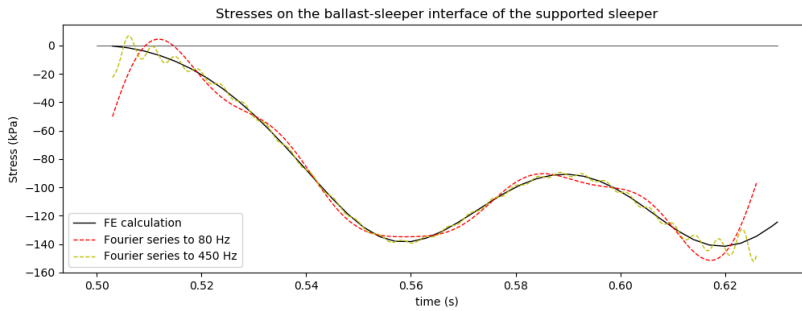


Figure 7.1: Sleeper-ballast interface stresses on supported sleeper from FE model and as Fourier series expansion

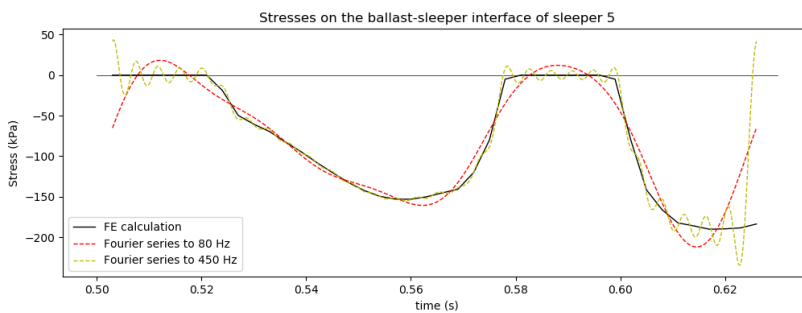


Figure 7.2: Sleeper-ballast interface stresses on hanging sleeper from FE model and as Fourier series expansion

7.2. First a function is constructed for  $n$  running up to 30, this led to frequencies up to 450 Hz, the result is plotted in yellow dashed lines. The corresponding frequency domain plotted in figure 7.3 shows only frequencies up to 80 Hz make a significant contribution. Note the graph of the frequency domain adopts the average of the two situations. The red dashed plotted lines confirm the course of the stresses can indeed be simulated with frequencies up to 80 Hz.

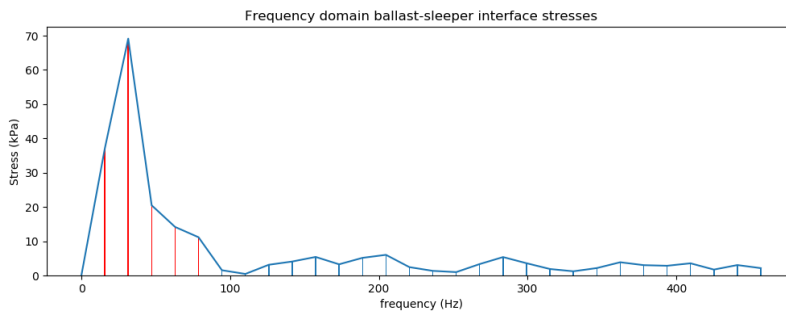


Figure 7.3: Frequency domain interface ballast-sleeper interface stresses

### 7.1.2. REQUIRED FEATURES

The calculations of the computational model are used to determine the expected range of the stresses to be measured at the ballast-sleeper interface. A factor 1.6 is adopted for rotation as explained in section 6.2. Also a certain margin of uncertainty is used due to doubts in the reliability of the calculations, that is, the stresses at the passage of the second axle do not match physics, as explained in section 4.2.2. However, since there is no reason to assume the stresses at the first axle passage are erroneous, the magnitude of the stresses is not expected to be of a much larger order, thus a small safety margin (10%) suffices. The required sampling frequency is set 8 times the maximal expected frequency in order to make sure the course of the stress will be captured well. It is known from experience that a factor 8 is sufficient for this (Hölscher, P., private communications). The required features for the ballast-sleeper interface measurement are listed in table 7.1.

Quantity	Range
Stress magnitude	0 to 350 kPa
Frequency domain	1 to 80 Hz
Sampling frequency	≥640 Hz

Table 7.1: Required features MBTSS ballast-sleeper interface

Tekscan model number 5250 is the most suitable sensor type offered for this measurement. Custom sensors can be designed as well, but that seems to expensive and costly for the benefit it brings since model 5250 meets all requirements listed in the table. The research of McHenry (2013) confirmed this sensor type to be the most suitable for ballast measurements. The instrument has a sensing area of 245.9 by 245.9 mm which is oriented diagonally from the tab, as shown in figure 7.4. The area comprises 44 rows and columns with each a row width of 3.3 mm and a span of 5.6 mm, that is a total of 1936 sensels. The sleeper soffit has an area of 300 by 2500 mm, meaning nine sensors can be positioned on the surface with an in between distance of 32 mm. This way not the whole of the surface will be covered but about 73%, the remaining surface stresses can be found by bridging the sensors with a proportional value. Since the contact points of the ballast particles are expected to distribute equally over the sleeper soffit (Abadi et al., 2015) this is not expected to lead to problems.

## 7.2. RAIL-SLEEPER INTERFACE

### 7.2.1. FREQUENCY DOMAIN

The stresses on the rail-sleeper interface are based on the train load adopted in the computational model, this is explained in section 4.1.7. This load is transformed into a Fourier series using the same formulas as describe in section 7.1.1, the result is plotted in figures 7.5 and 7.6. It is clear that the load can be simulated very well with a frequency domain up to 40 Hz.

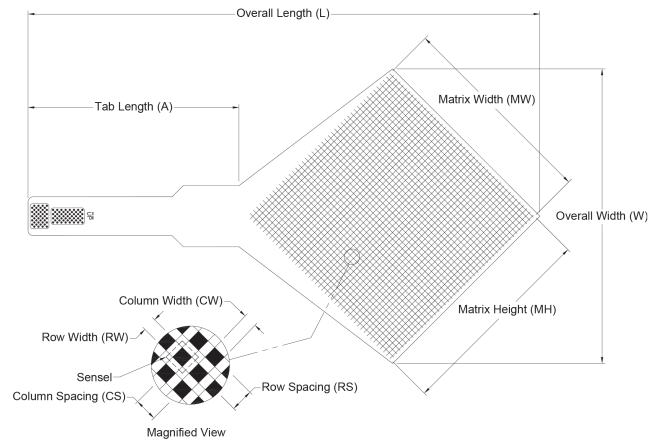


Figure 7.4: Tekscan 5250 sensor geometry (from Tekscan)

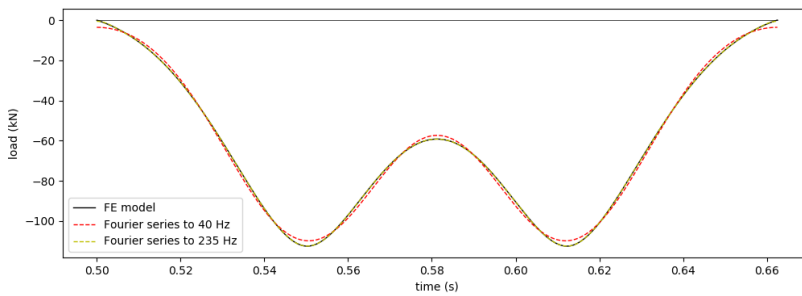


Figure 7.5: Vertical train load on sleeper from FE model and as Fourier series expansion

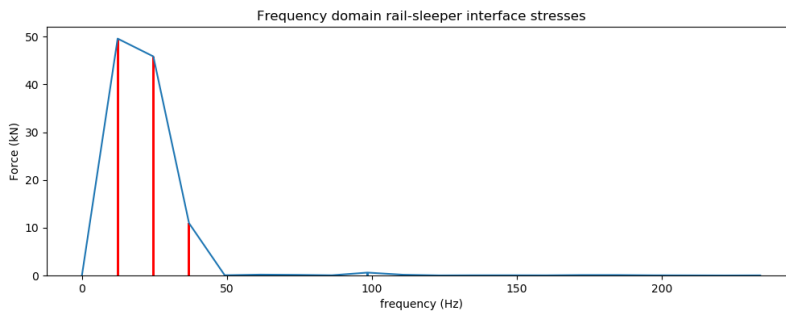


Figure 7.6: Frequency domain train load on sleeper

### 7.2.2. REQUIRED FEATURES

The required sampling frequency is again set to 8 times the expected maximal frequency. The magnitude of the train load is, based on the load applied in the computational model, up to 112.5 kN. In section 6.4 was explained how researches from Rapp et al. (2012) showed that the stresses are centered to a small area underneath the rail, which would lead to stresses up to 15000 kPa for an axle load of 225 kN. A larger value is recommended because of the safety margin and in because of the possibility of uneven axle loads. Table 7.2 lists the required characteristics of the MBTSS. This sensor has to take on much higher forces than those for the ballast-sleeper interface, because a similar load is transferred to a much smaller area. The area in between the bolts, that is the maximal surface where the forces are expected, is 95 by 304 mm<sup>2</sup>. The Tekscan type 5101 is able to measure a sufficiently high stress range and has a width of 112 mm, so two sensors can be placed next to each other underneath the baseplate.

Quantity	Range
Stress magnitude	0 to 15000 kPa
Frequency domain	1 to 40 Hz
Sampling frequency	≥320 Hz

Table 7.2: Required features MBTSS rail-sleeper interface

## 7.3. ACCELERATION MEASUREMENT

### 7.3.1. FREQUENCY DOMAIN

The vertical acceleration of a supported sleeper and a hanging sleeper are calculated with the computational model, as explained in 4.2.2, and are plotted in figures 7.7 and 7.8. The supported sleeper shows a relatively smooth line and a very small acceleration, because it is always resisted by the ballast. The hanging sleeper adopts a very high acceleration with some high peaks, because of the easy movement within the hanging distance. The sudden peaks make it difficult to simulate the acceleration with Fourier series, but the plots show all waves can be captured with frequencies up to 300 Hz (figure 7.9).

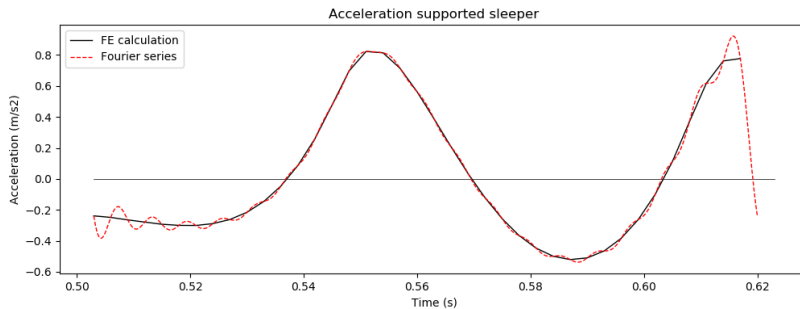


Figure 7.7: Vertical acceleration supported sleeper from FE model and as Fourier series expansion

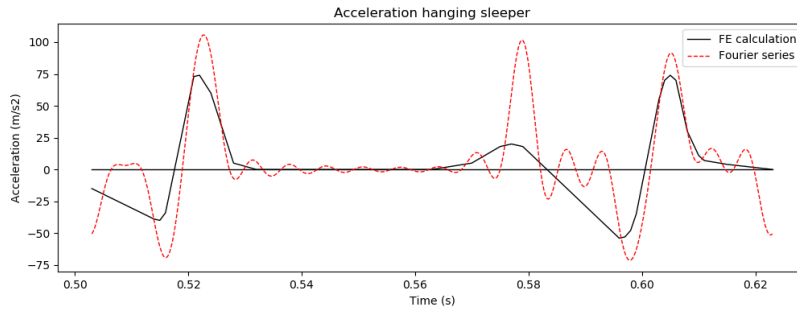


Figure 7.8: Vertical acceleration hanging sleeper from FE model and as Fourier series expansion

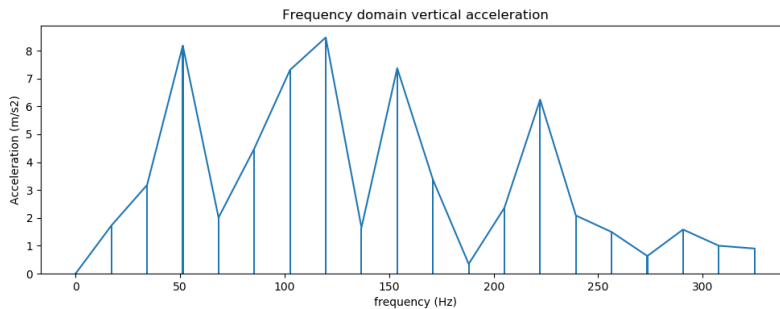


Figure 7.9: Frequency domain vertical acceleration sleeper

### 7.3.2. POSITIONING SENSORS

In order to determine the correct locations on the sleeper to measure the vertical acceleration, the deformations of the sleeper found in the calculations of the computational model are used. Figure 7.10 shows the deformed shapes of the sleeper in the two important modes that were found in the different calculations. The red crosses indicate the most suitable locations over the length of the sleeper; the position in the middle and at the outer ends makes sure the acceleration and the rotation of the sleeper will be captured. The positions at 0.4 meter from the outer ends, shown in figure 7.11, make sure the bending in the second mode is captured as well. Using these five positions reduces the consequences if one of the sensors will fail, because it will be still be possible to grasp the big picture with one of them falling out. The position of the sensor at the cross-section is not that relevant because the cross-section is not expected to rotate or deform, though for the sake of consistency it is recommended to place all sensors at the same height.

### 7.3.3. REQUIRED FEATURES

The required sampling frequency is 8 times the magnitude of the frequency domain. The range of magnitude of the acceleration is derived from calculations of the computational model described in 4.2.2. The instrument type can be chosen by using the requirements listed in table 7.3.

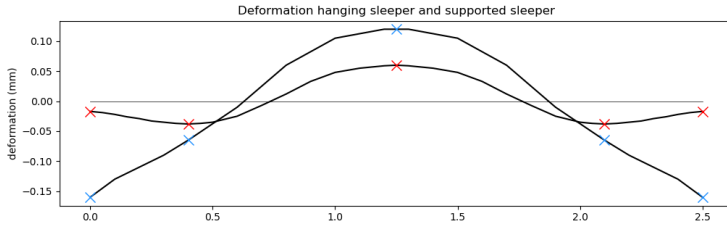


Figure 7.10: Deformation and positioning accelerometers over the length

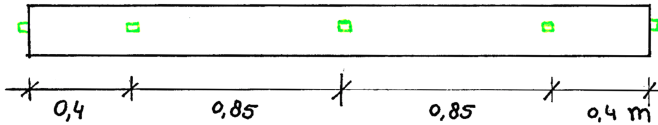


Figure 7.11: Position accelerometers

## 7.4. STRAIN MEASUREMENT

### 7.4.1. POSITIONING SENSORS

In the choices for the method of the strain measurement is made use of the calculations of the computational method as described in section 4.2.2. The expected moment distribution for the two calculated situations is plotted in figure 7.12, though some uncertainty margin is taken into account because of the doubts in the calculations. Since the graph clearly shows three peaks in the moment distribution, the moment should at least be determined at these three cross-sections. The location of these peaks can deviate at small changes in the stress distribution. It is therefore recommended to use Fiber Bragg Grating for the strain measurement, because this method allows for multiple measurements in a row and thereby makes sure the peaks in the moment distribution are captured. If it is decided to not perform strain measurements on the whole of the length, or if strain gauges will be used, it is important that the strain is measured at the locations where the moment peaks are expected. These locations are in the middle and at a distance of 0.5 meters from the ends, as shown in figure 7.13.

### 7.4.2. REQUIRED FEATURES

The calculations of the computational model showed a maximal moment of 6 kNm. Due to the uncertainty of this part of the calculation, a maximal value of 10 kNm is assumed.

Quantity	Range
Acceleration magnitude	-150 to 150 m/s <sup>2</sup>
Frequency domain	1 to 250 Hz
Sampling frequency	≥2000 Hz

Table 7.3: Required features accelerometers

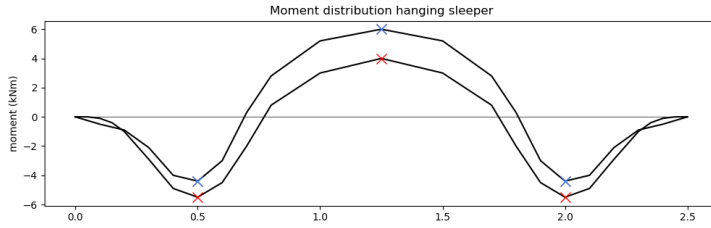


Figure 7.12: Moment distribution and positioning strain sensors over the length

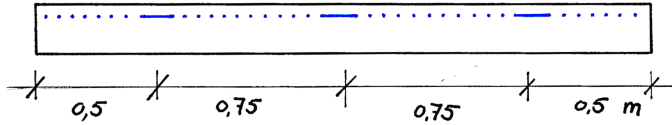


Figure 7.13: Position strain sensors

The maximal strain can be calculated using basic structural mechanics:

$$W = \frac{1}{6}bh^2 = \frac{1}{6} \cdot 0.289 \cdot 0.2^2 = 1.927 \cdot 10^{-3} [\text{m}^3] \quad (7.3)$$

$$\sigma = \frac{M}{W} = \frac{10 \cdot 10^3}{1.927 \cdot 10^{-3}} = 3.114 \cdot 10^6 [\text{N}/\text{m}^2] \quad (7.4)$$

$$\varepsilon = \frac{\sigma}{E} = \frac{3.114 \cdot 10^6}{3.7278 \cdot 10^{10}} = 83.5 \cdot 10^{-6} [-] \quad (7.5)$$

The frequency domain and the required sampling frequency of the sensor is based on the frequency of the stresses on the sleeper, described earlier in this chapter, because these are expected to behave in a similar frequency domain. The required features are listed in table 7.4.

Quantity	Range
Stress magnitude	-100 to 100 $\mu\epsilon$
Frequency domain	1 to 80 Hz
Sampling frequency	$\geq 640$ Hz

Table 7.4: Required features strain sensors

## 7.5. CONCLUSION

The required features of all measurement instruments are summarized in table 7.5. Based on these requirements it is recommended for the ballast-sleeper interface measurement to use the Tekscan type number 5250 and for the rail-sleeper interface use the Tekscan type number 5101. The choice of the instrument type for the strain measurement and

the acceleration measurement is left to the executors of the measurement, as this is expected to be a more economical and practical choice.

Instrument	Measurement range	Frequency domain	Sampling frequency
MBTSS (sleeper-ballast)	0 to 350 kPa	1 to 80 Hz	$\geq 640$ Hz
MBTSS (sleeper-rail)	0 to 15000 kPa	1 to 40 Hz	$\geq 320$ Hz
Accelerometer	-150 to 150 m/s <sup>2</sup>	1 to 250 Hz	$\geq 2000$ Hz
Strain sensor	-100 to 100 $\mu\epsilon$	1 to 80 Hz	$\geq 640$ Hz

Table 7.5: Overview required features



# 8

## CONCLUSION

### COMPUTATIONAL MODEL

This report firstly describes a method to analyze the behaviour of one single sleeper in a transition zone using a finite element model in an open source software package named Kratos. Linear material behaviour was assumed for the ballast and sleeper elements, which seems suitable when looking only at the dynamic behaviour of a sleeper during a single train passage.

To simulate the force of the rail ‘pulling’ the sleeper back to its initial state, the sleeper was fixed to linear elastic springs at the top side of the model. The stiffness of this springs was based on the bending stiffness of the rail and the expected behaviour of surrounding sleepers. It turned out the stiffness of the rail is so high that the main parameter for the rail resistance is the displacement of the surrounding sleepers. Following this line of reasoning, the displacement of each sleeper is highly interdependent as well as it depends on time and degradation of the track, which makes it very difficult to capture this force in one linear spring. Although the method presented in this report is expected to be the best way to simulate the rail resistance for an individual sleeper, it must be concluded that it is not possible to simulate the behaviour of a sleeper properly when looking at one individual sleeper only. A larger part of the railway must be modelled in order to be able to predict the interrelationships of the sleepers.

In order to simulate the hanging distance, interface elements were used in between the ballast and the sleeper. The elements were activated only when the two bodies showed physical contact, to then adopt a very high stiffness so that the two bodies will not (or as little as possible) interpenetrate. The interface elements adopted Mohr-Coulomb criteria in order to allow for shear movements at the interface. Although this method suffices in theory, it turned out to be very difficult to implement in FE software. Despite multiple adjustments in collaboration with the Kratos software engineer, calculations often failed to converge and it wasn’t possible to run a calculation as desired.

### DESIGN MEASUREMENT SLEEPER

The best way to measure the vertical stresses at the ballast-sleeper interface is by means of the matrix based tactile surface sensor (MBTSS), that is a thin mat that is able to measure the stress distribution on this surface over time with a very high frequency. Tekscan manufactures surface sensors that have proved suitable for railway measurements. Sufficient protection against damage is needed when these sensor are fixed at the sleeper soffit, which can be provided by an under sleeper pad. An important problem with this measurement method is the calibration of the sensor for this type of stress distribution, that is, it is so far not succeeded to find a solid solution for this. Close attention will have to be paid to this in advance of a field-measurement, though it can not be ruled out that it won't be possible to calibrate the sensors properly. It is for that reason that extra measurements are necessary to validate the magnitude of the measured stresses.

The first validation can be realised by equating the sum of the vertical forces to the mass of the sleeper times its vertical acceleration. The vertical stresses on top can be measured by using again the MBTSS at the rail-sleeper interfaces. Accelerometers will have to be placed on the sleeper to measure the acceleration. The second validation can be performed by strain measurements at multiple locations along the length of the beam. This way the moment distribution can be determined and conformed to the force distribution over the length of the ballast-sleeper interface.

### RECOMMENDATION

The prescribed features of the measuring instruments are largely based on the calculations of the computational model, but as previously described, there are errors in the model. This data will therefore have to be studied in more detail to be sure that all values are correct. If more in-depth calculations are desired, it is advised to build the model in a different way, preferably considering a larger railway section and not only one individual sleeper. If one chooses to use a similar interface method, the FE script requires a great deal of improvement.

A major challenge in performing the ballast-sleeper interface measurement is the calibration of the MBTSS. It is expected that the core of this problem lies in the distribution of the stresses over the sensels. Because of the angular shape of the ballast particles the stresses are often brought together to very small contact points, which might not be captured because they get lost between the sensels. It is expected that an under sleeper pad will spread out these contact points sufficiently, though this will eventually have to be checked in laboratory tests. If it turns out that the under sleeper pad does not spread the forces sufficiently, a stiffer layer to cover the sensor can be considered.

## REFERENCES

- Paikowsky, S.G., and Hadjuk, E.L. (1997). Calibration and use of grid-based tactile pressure sensors in granular material. *Geotechnical Testing Journal*, 20(2), 218-241. <https://doi.org/10.1520/GTJ10741J>
- Dahlberg, T. (2004). Railway track settlements - a literature overview. Report for the EU project SUPERTRACK, 2004.
- Stith, J.C. and Rose, J.G. (2004). Pressure measurements in railroad trackbeds at the rail/tie interace using Tekscan sensors. 2017 Joint Rail Conference. <https://doi.org/10.1115/JRC2017-2219>
- Stith, J.C. (2005). Railroad track pressure measurements at the rail/tie interface using telscan sensors. [Master's thesis, University of Kentucky]. [https://uknowledge.uky.edu/gradschool\\_theses/213](https://uknowledge.uky.edu/gradschool_theses/213)
- Holscher, P., and Meijers, P. (2009). Analysis of track and soil behavior at transition zones. Delft Cluster, 2009.
- Palmer, M.C., O'Rourke, T/ D., Olson, N.A., Abdoun, T., Ha, D., O'Rourke, M.J. (2009). Tactile pressure sensors for soil-structure interaction assessment. *Journal of Geotechnical and geoenvironmental engineering*, 135(11), 1638-1645. [https://doi.org/10.1061/\(ASCE\)GT.1943-5606.0000143](https://doi.org/10.1061/(ASCE)GT.1943-5606.0000143)
- Coelho, B., Hölischer, P. (2010). An assessment of transition zone performance. *Proceedings of the Institution of Mechanical Engineers Part F Journal of Rail and Rapid Transit*, 1(F2), 1-11. <https://doi.org/10.1243/09544097JRRT389>
- Coelho, B. (2011). Dynamica of railway transition zones in soft soils. [PhD thesis, Delft University of Technology]. TU Delft Repository. <https://repository.tudelft.nl/islandora/object/uuid%3A950e7ccd-1b18-4530-866d-5dd662fe0fa4>
- Rapp, C.T., Dersch, M.S., Edwards, J.R., Barkan, C.PL., Wilson, B., and Mediavilla, J. (2012). Measuring concrete crosstie rail seat pressure distribution with matrix based tactile surface sensors. 2012 Joint Rail Conference, 85-92. <https://doi.org/10.1115/JRC2012-74092>
- McHenry, M.T. (2013). Pressure measurement at the ballast-tie interface of railroad track using matrix based tactile surface sensors. [Master's thesis, University of Kentucky]. <https://doi.org/10.3141%2F2476-04>
- Varandas, J.N. (2013). Long-term behaviour of railway transitions under dynamic loading. [PhD thesis, NOVA University Lisbon].

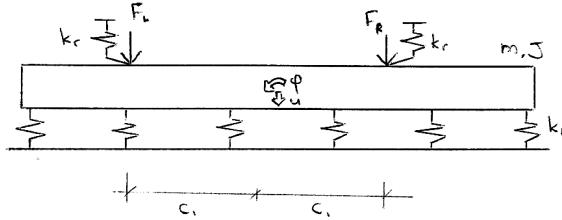
- Ferdous, W., Manalo, A. (2014). Failures of mainline railway sleepers and suggested remedies - review of current practice. *Engineering Failure Analysis*, 44, 17-35. <http://dx.doi.org/10.1016/j.engfailanal.2014.04.020>
- Abadi, T., Le Pen, L., Zervos, A., and Powerie, W. (2015). Measuring the area and number of ballast particle contacts at sleeper/ballast and ballast/subgrade interfaces. *International Journal of Railway Technology*, 4(2), 45-72. <https://doi.org/10.4203/ijrt.4.2.3>
- Massaroni, C., Saccomandi, P., and Schena, E. (2015). Medical smart textiles based on fiber optic technology: an overview. *Journal of Functional Biomaterials*, 6(2), 204-221. <https://doi.org/10.3390/jfb6020204>
- Rose, J.G., Stark, T.D., Wilk, S.T., and Purcell, M. (2015). Design and monitoring of well-performing bridge transitions. 2015 Joint Rail Conference. <https://doi.org/10.1115/JRC2015-5645>
- Grabe, P.J., Mtshotana, B.F., Sebati, M.M., and Thunemann, E.Q. (2016). The effect of under-sleeper pads on sleeper-ballast interaction. *Journal of the South African Institution of Civil Engineering*, 58(2), 35-41. <https://doi.org/10.17159/2309-8775/2016/v58n2a4>
- Varandas, J.N., Holscher, P., and Silva, M.A.G. (2016). Three-dimensional track-ballast interaction model for the study of a culvert transition. *Soil Dynamics and Earthquake Engineering*, 89, 116-127. <http://dx.doi.org/10.1016/j.soildyn.2016.07.013>
- Edwards, J.R., Gao, Z., Wolf, H.E., Dersch, M.S., and Qian Y. (2017). Quantification of concrete railway sleeper bending moments using surface strain gauges. *Measurement*, 111, 197-207. <http://dx.doi.org/10.1016/j.measurement.2017.07.029>
- Gao, Z., Qian, Y., Dersch, M., and Edwards, J.R. (2017). Compressive stress distribution in prestressed concrete and its effect on railroad cross-tie design. *Construction and Building Materials*, 151, 147-157. <http://dx.doi.org/10.1016/j.conbuildmat.2017.05.186>
- Rose, J.G., Purcell, M.L., Liu, Q., and Lei, X. (2017). Pressure measurements at the tie-ballast interface in railroad tracks using granular material pressure cells. 2017 Joint Rail Conference. <https://doi.org/10.1177%2F0361198118775872>
- Heydari-Noghabi, H., Varandas, J.N., Esmaeli, M., and Zakeri, J. (2017). Investigating the influence of auxiliary rails on dynamic behavior of railway transition zone by a 3D train-track interaction model. *Latin American Journal of Solids and Structures*, 14(11), 2000-2018. <http://dx.doi.org/10.1590/1679-78253906>
- Ngamkhanong, C., Kaewunruen, S., and Afonso Costa, B.J. (2018). State-of-the-art review of railway track resilience monitoring. *Infrastructures*, 3(1), 3. <https://doi.org/10.3390/infrastructures3010003>
- Paião, A., Varandas, J.N., Fortunato, E., and Calcada, R. (2018). Numerical simulations to improve the use of under sleeper pads at transition zones to railway bridges. *Engineering Structures*, 164, 169-182. <https://doi.org/10.1016/j.engstruct.2018.03.005>

- 
- Watts, T.J. (2018). Direct measurement of crosstie-ballast interface pressures using granular material pressure cells. [Master's thesis, University of Kentucky]. Semantic Scholar. <https://doi.org/10.13023/etd.2018.440>
- Tran, L., Hoang, T., Foret, G., Duhamel, D., Messad, S., and Loaec, A. (2020). Identification of train loads from the dynamic responses of an integrated sleeper in situ. *Journal of Intelligent Material Systems and Structures*, 31(11). <https://doi.org/10.1177%2F1045389X20922905>
- Varandas, J.N., Paião, A., Fortunato, E., Coelho, B., and Holscher, P (2020). Long-term deformation of railway tracks considering train-track interaction and non-linear resilient behavior of aggregates - a 3D FEM implementation. *Computers and Geotechnics*, 126. <https://doi.org/10.1016/j.compgeo.2020.103712/>



# A

## ANALYTIC CALCULATION



**Sum vertical forces:**

$$\underbrace{F_L - k_r \cdot (u + c_1 \cdot \varphi)}_{\text{left rail}} + \underbrace{F_R - k_r \cdot (u - c_1 \cdot \varphi)}_{\text{right rail}} - \underbrace{\int_L k_b \cdot (u - \varphi \cdot x) dx}_{\text{ballast}} = m \cdot \ddot{u} \quad (\text{A.1})$$

$$\int_L k_b \cdot (u - \varphi \cdot x) dx = k_b \cdot \left[ u \cdot x - \frac{1}{2} \varphi x^2 \right]_{-L/2}^{L/2} = k_b \cdot u \cdot L \quad (\text{A.2})$$

$$\begin{aligned} F_L - k_r \cdot (u + c_1 \cdot \varphi) + F_R - k_r \cdot (u - c_1 \cdot \varphi) - k_b \cdot u \cdot L &= m \cdot \ddot{u} \\ F_L + F_R - (2 \cdot k_r + k_b \cdot L) \cdot u &= m \cdot \ddot{u} \\ m \cdot \ddot{u} + (2 \cdot k_r + k_b \cdot L) \cdot u &= F_L + F_R \end{aligned} \quad (\text{A.3})$$

**Sum rotational moment:**

$$\underbrace{c_1 \cdot (F_L - k_r \cdot (u + c_1 \cdot \varphi))}_{\text{left rail}} + \underbrace{c_1 \cdot (F_R - k_r \cdot (u - c_1 \cdot \varphi))}_{\text{right rail}} + \underbrace{\int_L k_b \cdot x \cdot (u - \varphi \cdot x) dx}_{\text{ballast}} = J \cdot \ddot{\varphi} \quad (\text{A.4})$$

$$\int_L k_b \cdot x \cdot (u - \varphi \cdot x) dx = k_b \cdot \left[ \frac{1}{2} u \cdot x^2 - \frac{1}{3} \varphi \cdot x^3 \right]_{-L/2}^{L/2} = -\frac{1}{12} k_b \cdot L^3 \cdot \varphi \quad (\text{A.5})$$

$$\begin{aligned} c_1 \cdot (F_L - k_r \cdot (u + c_1 \cdot \varphi)) - c_1 \cdot (F_R - k_r \cdot (u - c_1 \cdot \varphi)) + k_b \cdot \int_L x \cdot (u - \varphi \cdot x) dx &= J \cdot \ddot{\varphi} \\ c_1 \cdot F_L - c_1 \cdot F_R - 2 \cdot c_1^2 \cdot k_r \cdot \varphi - k_b \cdot \frac{1}{12} L^3 \varphi &= J \cdot \ddot{\varphi} \quad (\text{A.6}) \\ J \cdot \ddot{\varphi} + (2 \cdot c_1^2 \cdot k_r + k_b \cdot \frac{1}{12} L^3) \varphi &= c_1 \cdot F_L - c_1 \cdot F_R \end{aligned}$$

**Combining:**

$$\begin{bmatrix} m & 0 \\ 0 & J \end{bmatrix} \begin{bmatrix} \ddot{u} \\ \ddot{\varphi} \end{bmatrix} + \begin{bmatrix} 2k_r + k_b L & 0 \\ 0 & 2c_1^2 k_r + \frac{1}{12} k_b L^3 \end{bmatrix} \begin{bmatrix} u \\ \varphi \end{bmatrix} = \begin{bmatrix} F_L + F_R \\ c_1 \cdot (F_L - F_R) \end{bmatrix} \quad (\text{A.7})$$

**General solution:**

$$\begin{aligned} m\ddot{x} + kx &= F \sin(\omega t) \\ x_h &= A \sin(\omega_n t) + B \cos(\omega_n t) \\ x_p &= \frac{F}{k - m\omega^2} \sin(\omega t) \\ x(t) &= A \sin(\omega_n t) + B \cos(\omega_n t) + \frac{F}{k - m\omega^2} \sin(\omega t) \\ x(0) = B = 0 &\rightarrow x(t) = A \sin(\omega_n t) + \frac{F}{k - m\omega^2} \sin(\omega t) \\ \dot{x}(t) &= A \omega_n \cos(\omega_n t) + \frac{\omega F}{k - m\omega^2} \cos(\omega t) \\ \dot{x}(0) = A \omega_n + \frac{\omega F}{k - m\omega^2} = 0 &\rightarrow A = -\frac{\omega F}{\omega_n (k - m\omega^2)} \\ x(t) &= -\frac{\omega F}{\omega_n (k - m\omega^2)} \sin(\omega_n t) + \frac{F}{k - m\omega^2} \sin(\omega t) \\ x(t) &= \frac{F}{k - m\omega^2} \left( \sin(\omega t) - \frac{\omega}{\omega_n} \sin(\omega_n t) \right) \end{aligned} \quad (\text{A.8})$$

note:

$x_h$  = homogeneous solution

$x_p$  = particular solution

$\omega_n = \sqrt{\frac{k}{m}}$  = eigenfrequency

**Solution Displacement:**

$$\begin{aligned}
 m\ddot{u} + (2k_r + k_b L)u &= (F_L + F_R)\sin(\omega t) \\
 \omega_n &= \sqrt{\frac{2k_r + k_b L}{m}} \\
 u(t) &= \frac{F_L + F_R}{2k_r + k_b L - m\omega^2} \left( \sin(\omega t) - \frac{\omega}{\omega_n} \sin(\omega_n t) \right)
 \end{aligned} \tag{A.9}$$

**Solution Rotation:**

$$\begin{aligned}
 J\ddot{\varphi} + (2c_1^2 k_r + \frac{1}{12} k_b L^3)\varphi &= (c_1 F_L - c_1 F_R)\sin(\omega t) \\
 \omega_n &= \sqrt{\frac{2c_1^2 k_r + \frac{1}{12} k_b L^3}{J}} \\
 \varphi(t) &= \frac{c_1 (F_L - F_R)}{2c_1^2 k_r + \frac{1}{12} k_b L^3 - J\omega^2} \left( \sin(\omega t) - \frac{\omega}{\omega_n} \sin(\omega_n t) \right)
 \end{aligned} \tag{A.10}$$

**Parameters**

$$\begin{aligned}
 c_1 &= 0.72 \text{ m} \\
 k_b &= 0.3 \cdot 1.8 \cdot 10^3 \text{ N/m} \\
 J &= 192.2 \text{ kgm}^2 \\
 L &= 2.5 \text{ m} \\
 m &= 369 \text{ kg}
 \end{aligned}$$